

Loss of DP1 Aggravates Vascular Remodeling in Pulmonary Arterial Hypertension via mTORC1 Signaling

Yuhu He^{1,2,3*}, Caojian Zuo^{3,4}, Daile Jia^{3,5*}, Peiyuan Bai^{3,5*}, Deping Kong^{1*}, Di Chen^{3*}, Guizhu Liu⁶, Juanjuan Li³, Yuanyang Wang¹, Guilin Chen¹, Shuai Yan³, Bing Xiao³, Jian Zhang¹, Linjuan Piao³, Yanli Li¹, Yi Deng¹, Bin Li⁷, Philippe P. Roux⁸, Katrin I. Andreasson⁹, Richard M. Breyer¹⁰, Yunchao Su¹¹, Jian Wang^{6†}, Ankang Lyu^{5†}, Yujun Shen^{1†}, Ying Yu^{1,3,6†}

¹Department of Pharmacology, Tianjin Key Laboratory of Inflammation Biology, Key Laboratory of Immune Microenvironment and Disease (Ministry of Education), School of Basic Medical Sciences, Tianjin Medical University, Tianjin, China

²Department of Cardiovascular Medicine, The Second Xiangya Hospital, Central South University, Changsha, Hunan, China

³CAS Key Laboratory of Nutrition, Metabolism and Food Safety, Shanghai Institute of Nutrition and Health, Shanghai Institutes for Biological Sciences, University of Chinese Academy of Sciences, Chinese Academy of Sciences, Shanghai, China

⁴Department of Cardiology, Shanghai General Hospital, School of Medicine, Shanghai Jiaotong University, Shanghai, China

⁵Department of Cardiology, Ruijin Hospital, Shanghai Jiaotong University School of Medicine, Shanghai, China

⁶State Key Laboratory of Respiratory Diseases, Guangzhou Institute of Respiratory Health,

The First Affiliated Hospital of Guangzhou Medical University, Guangzhou, Guangdong, China

⁷Orthopedic Institute, Soochow University, Jiangsu, China

⁸Institute for Research in Immunology and Cancer, and Department of Pathology and Cell Biology, Université de Montréal, Montreal, QC, Canada

⁹Department of Neurology and Neurological Sciences, Stanford University School of Medicine, Stanford, CA, USA

¹⁰Department of Veterans Affairs, Tennessee Valley Health Authority, and Department of Medicine, Vanderbilt University Medical Center, Nashville, TN, USA

¹¹Department of Pharmacology and Toxicology, Medical College of Georgia, Augusta University, Augusta, GA, USA

*These authors contributed equally to this article.

†Correspondence to:

Ying Yu, MD, PhD or Yujun Shen, PhD

Department of Pharmacology, School of Basic Medical Sciences, Tianjin Medical University, 22 Qixiangtai Rd, Heping District, Tianjin 300070, China

E-mail: yuying@tmu.edu.cn (YY) or yujun_shen@tmu.edu.cn (YS)

Ankang Lyu, MD, PhD

Department of Cardiology, Ruijin Hospital, Shanghai Jiaotong University School of Medicine, 197 Ruijin 2nd Road, Luwan District, Shanghai 200025, China

E-mail: lvankangrj@163.com

Jian Wang, MD, PhD

State Key Laboratory of Respiratory Disease, The First Affiliated Hospital, Guangzhou Medical University, 151 Yanjiang Road, Guangzhou, Guangdong, China

E-mail: jianwang1@email.arizona.edu

Author contributions:

Y. He, J. Wang, A. Lyu, Y. Shen, Y. Yu designed research. Y. He, Y. Shen, and Y. Yu wrote the paper. Y. He, C. Zuo, D. Jia, P. Bai, G. D. Kong, D. Chen, Liu, Y. Wang, G. Chen, S. Yan, B. Xiao, J. Li, and B. Li conducted experiments. J. Zhang, L. Piao, D. Kong, J. Wang, A. Lyu, Y. Shen, and Y. Yu analyzed the data. P.P. Roux, K.I. Andreasson, R.M. Breyer, and Y. Su provided important reagents and tissue samples.

Grant support:

This work was supported by the National Key R&D Program of China (no. 2017YFC1307404), National Natural Science Foundation of China (nos. 81790623, 81525004, 91439204, 81930002, 81630004 and 81800059), Natural Science Foundation of Tianjin(no. 17JCYBJC40700) and US NIH grants (HL134895, HL115078 and HL134934). Y. Yu is a Fellow at the Jiangsu Collaborative Innovation Center for Cardiovascular Disease Translational Medicine.

Running title: DP1 and pulmonary arterial hypertension

Subject code: 17.6/ 3.15/ 17.10

At a Glance Commentary

Scientific Knowledge on the Subject:

Pulmonary arterial hypertension (PAH) is a devastating disease characterized by pulmonary vascular remodeling such as smooth muscle cell (SMC) hypertrophy and proliferation. Prostaglandin (PG) I₂ analogs (baraprost, iloprost, and treprostinil) are effective in the treatment of PAH. PGD₂ exerts pro-resolution and vasodilatory effects via D prostanoid receptor subtype 1 (DP1). Treprostinil is also a potent DP1 agonist. It remains unknown whether the clinically favorable effects of treprostinil in severe PAH is attributable to concomitant activation of DP1 receptor.

What This Study Adds to the Field:

In this study, we demonstrate that DP1 expression was downregulated in pulmonary arteries (PAs) in various animal models of PAH and idiopathic PAH patients. Ablation of DP1 receptor exacerbated hypoxia-induced PAH and enhances PA remodeling in mice through activation of mTORC1 signaling. DP1 activation facilitated mTORC1 complex dissociation and suppresses mTORC1 activity in PASMCs through protein kinase A -dependent phosphorylation of raptor at Ser791. We also found that treprostinil possessed therapeutic effects on PAH in mice in part through DP1 receptor. These findings suggest that DP1 receptor is a potential therapeutic target for PAH treatment.

This article has an online data supplement, which is accessible from this issue's table of content online at www.atsjournals.org

Abstract

Rationale: Vascular remodeling, including smooth muscle cell hypertrophy and proliferation, is the key pathological feature of pulmonary arterial hypertension (PAH). Prostaglandin (PG) I₂ analogs (baraprost, iloprost, and treprostinil) are effective in the treatment of PAH. Of note, the clinically favorable effects of treprostinil in severe PAH may be attributable to concomitant activation of PGD₂ receptor subtype 1 (DP1).

Objectives: To study the role of DP1 in the progression of PAH and its underlying mechanism.

Methods and Results: DP1 expression was downregulated in hypoxia-treated PASMCs and in pulmonary arteries (PAs) from rodent PAH models and idiopathic PAH patients. *DPI* deletion exacerbated PA remodeling in hypoxia-induced PAH, whereas pharmacological activation or forced expression of DP1 receptor had the opposite effect in different rodent models. *DPI* deficiency promoted PASMC hypertrophy and proliferation in response to hypoxia via induction of mammalian target of rapamycin complex (mTORC) 1 activity. Rapamycin, an inhibitor of mTORC1, alleviated the hypoxia-induced exacerbation of PAH in *DP1*^{-/-} mice. DP1 activation facilitated raptor dissociation from mTORC1 complex and suppressed mTORC1 activity through protein kinase A (PKA)-dependent phosphorylation of raptor at Ser791. Moreover, treprostinil treatment blocked the progression of hypoxia-induced PAH in mice in part by targeting DP1 receptor.

Conclusion: DP1 activation attenuates hypoxia-induced PA remodeling and PAH through PKA-mediated dissociation of raptor from the mTORC1 complex. These results suggest that

DP1 receptor may serve as a therapeutic target for the management of PAH.

Keywords: pulmonary arterial hypertension; DP 1 receptor; pulmonary arterial smooth muscle cell; hypertrophy and proliferation; mTOR signaling.

Introduction

Pulmonary arterial hypertension (PAH) is a progressive and lethal pulmonary vascular disease characterized by severe distal pulmonary artery (PA) remodeling and increased pulmonary vascular resistance that eventually leads to right-side heart failure. Endothelial dysfunction, smooth muscle cell hyperplasia and hypertrophy, extracellular matrix deposition, and perivascular inflammatory infiltrate contribute to PA remodeling in PAH(1). Current available therapies such as endothelin receptor antagonists, phosphodiesterase inhibitors, and prostacyclin analogs predominantly target pulmonary vasoconstriction and improve PAH symptoms, but the mortality rate remains unsatisfactory. Identifying novel pathways involved in pulmonary vascular remodeling can reveal novel therapeutic targets, which can lead to improved clinical outcomes(2).

Arachidonic acid metabolites play a critical role in maintaining pulmonary vascular homeostasis. Cyclooxygenase (COX) catalyzes the transformation of arachidonic acid into prostaglandins (PGs) including PGE₂, PGD₂, PGF_{2α}, and PGI₂ (prostacyclin), and thromboxane (Tx), all of which exert their (patho)physiological functions through activation of the cognate G protein-coupled receptor (i.e., PGE₂ receptor [EP]1–4, PGD₂ receptor (DP)1 and DP2, PGF_{2α} receptor, PGI₂ receptor [IP], and thromboxane receptor). Loss of COX-2 exacerbates hypoxia-induced PAH in mice by increasing vascular smooth muscle cell (VSMC) contractility(3). In clinic, PGI₂ analogs and IP receptor agonists are widely used to manage PAH. Currently employed IP agonists include synthetic PGI₂ (epoprostenol), stable PGI₂ analogs (baraprost, iloprost, and treprostinil), and a highly selective IP agonist

(selexipag)(4). Like endogenous PGI₂, synthetic epoprostenol is unstable at room temperature and has a very short half-life. In contrast, selexipag—which is chemically distinct from PGI₂—is an orally delivered, potent non-prostanoid IP receptor agonist(5). As an inhaled medication, treprostinil exerts a more sustained effect on pulmonary vascular resistance with higher tolerability at relatively low doses than iloprost(6), and clinical observations have shown that transitioning from inhaled iloprost to treprostinil markedly improves quality of life in PAH patients(7).

The three analogs have heterogeneous binding affinities for other PG receptors, which may confer variable clinical efficacy(8, 9). For example, non-specific binding and activation of EP3 receptor could decrease the long-term tolerability and efficacy of PGI₂ analogs(10, 11). Despite a longer half-life, treprostinil has much higher affinity for the vasodilator DP1 and EP2 receptors than iloprost(9). DP1 is expressed in both human PAs and veins and its activation induces relaxation of human pulmonary vessels(12); on the other hand, EP2 suppresses endothelin-1-stimulated proliferation of human PA smooth muscle cells in vitro(13). Thus, DP1 antagonists inhibit the relaxation of human PAs induced by treprostinil, suggesting that it could mediate the therapeutic effects of treprostinil in PAH patients(14). However, whether DP1 and EP2 receptors are involved in the pathogenesis of PAH remains to be determined.

In this study, we demonstrate that DP1 expression is downregulated in PAs in various animal models of PAH and idiopathic PAH patients. Ablation of DP1 receptor exacerbated hypoxia-induced PAH in mice by enhancing mammalian target of rapamycin complex

(mTORC) 1 activity. We also found that treprostinil exerts therapeutic effects on PAH in mice in part through DP1. These findings suggest that DP1 is a potential therapeutic target for PAH treatment.

Methods

Extended description of the materials and methods is provided in the online supplement.

Animals

8 to 10-week-old male mice and rats were used in all experiments in this study. Wild-type (WT), IP knockout ($IP^{-/-}$), *DP1* knockout ($DP1^{-/-}$), and *EP2* knockout ($EP2^{-/-}$) mice were maintained on a C57BL/6 genetic background. $DP1^{-/-}$ and $IP^{-/-}$ mice were mated to generate the double knockout ($DP1^{-/-} IP^{-/-}$) mice. VSMC -specific DP1-KO mice ($DP1^{F/F}SM22^{Cre}$) were generated by crossing $DP1^{F/F}$ mice(15) with SM22-Cre transgenic mice(10). WT littermates of each strain were generated as experimental controls by mating heterozygotes. Mice were maintained in an environment with controlled temperature ($22^{\circ}\text{C} \pm 1^{\circ}\text{C}$) and relative humidity ($50\% \pm 5\%$) on a 12:12-h light/dark cycle, with free access to sterile food and water. Animal experiments were approved by the Institutional Animal Care and Use Committee of the Institute for Nutritional Sciences, University of Chinese Academy of Sciences.

Rodent models of PAH

A hypoxia- or hypoxia + SU5416 (HySU)-induced mouse model of PAH and a monocrotaline (MCT)-induced rat model of PAH were used to examine PAH development.

In all animal experiments, littermates or vehicle-treated animals were used as controls. For the hypoxia-induced PAH model, 8- to 10- week-old male mice maintained on normal chow were exposed to 10% O₂ (hypoxia) or room air (normoxia) for 3 weeks as previously described(10). To restore DP1 expression, 1 week before hypoxia induction, lentivirus encoding DP1 (3×10^8 transduction units in 30 μ l phosphate-buffered saline [PBS]) was injected into the trachea of DP1^{-/-} mice followed by injection of air to promote the spread of virus throughout the lungs(16). For rapamycin treatment, mice were intraperitoneally injected with rapamycin at 3 mg/kg every other day during the 3-week hypoxia exposure period(17).

For the HySU model, mice were subcutaneously injected with the vascular endothelial growth factor receptor inhibitor SU5416 (20 mg/kg body weight) under isoflurane anesthesia followed by exposure to hypoxia (10% O₂) for 3 weeks according to a previous report(18). An Alzet osmotic mini-pump (DURECT Corporation, Cupertino, CA, USA) filled with either treprostinil (infusion rate: 30 ng·kg⁻¹·min⁻¹) or sterile 0.9% injectable saline and equilibrated at 37°C in PBS for 48 h was subcutaneously implanted into the mice(19), which were subjected to HySU treatment 3 days later.

At the end of the treatment, animals were anesthetized and a 1.2-F (for mice) or 1.4-F (for rats) micro-tip pressure transducer catheter (Millar Instruments, Houston, TX, USA) was carefully inserted into the right ventricle (RV), and RV systolic pressure (RVSP) was continuously monitored for 5 min using a PowerLab data acquisition system (ADInstruments, Sydney, Australia). RV hypertrophy was assessed by Fulton index measurements (weight of RV/weight of left ventricle plus septum [RV/LV+S]).

Statistical analysis

Data are expressed as mean \pm SEM and were analyzed using Prism v.5.0 software (GraphPad Inc., La Jolla, CA, USA). The two-tailed unpaired Student's *t* test and one- or two-way analysis of variance with a Bonferroni post-hoc test was used to compare the means of different groups. $P < 0.05$ was considered statistically significant. Randomization and blind analyses were used whenever possible.

Results

DP1 receptor is downregulated in PAs from PAH rodent models and idiopathic PAH patients

COX-2 expression is up-regulated in lung tissues from PAH patients and in PAs from mice with hypoxia-induced PAH(10, 20). Accordingly, we found that all PG products were upregulated in the lungs of mice in response to chronic hypoxia (Supplemental Figure E1a–e). *DPI* deficiency had no impact on PG generation. On the other hand, DP1, not DP2, mRNA expression was markedly reduced in PAs from chronic hypoxia-treated mice and MCT-treated rats (Figure 1a,b) and in mPASCs cultured under hypoxic conditions (Figure 1c), whereas DP2 expression was unchanged. Similarly, DP1 expression was downregulated in human (h)PASCs in response to hypoxia (Figure 1d). DP1 protein, mainly located in SMC layer (Figure 1e), was downregulated in PAs from hypoxia-treated mice (Figure 1e-f). Consistently, we also observed DP1 expression was reduced in PAs from idiopathic PAH patients as compared to healthy individuals (Figure 1g-h).

Then we explored the underlying mechanisms for hypoxia-induced DP1 downregulation using mouse VSMC line MOVAS (Supplemental Figure E2a). Multiple potential transcription factor binding motifs for HIF1 α , BCL6, Egr1 and Creb1 were predicted in DP1 gene promoter region using FindM software (Supplemental Figure E2b). Indeed, hypoxia increased the expression of the 4 transcription factors (Supplemental Figure E2c-f). However, knockdown of either HIF1 α or BCL6, not Creb1 and Egr1, markedly attenuated hypoxia-triggered DP1 downregulation in MOVAS cells (Supplemental Figure E2g-n). Through chromatin immunoprecipitation assay, we observed hypoxia treatment dramatically increased HIF1 α and BCL6 binding activity on DP1 promoter region at -3651~ -3636bp (Supplemental Figure E3a-c) and at -3826~ -3807bp, respectively (Supplemental Figure E3a, E3c). Interestingly, HIF1 α interacted with BCL6 each other in MOVAS cells (Supplemental Figure E3d-e). Thus, hypoxia suppressed DP1 expression in VSMCs probably through HIF1 α -mediated recruitment of inhibitory transcription factor BCL6 (Supplemental Figure E3f)

Deletion of DP1 but not EP2 exacerbates hypoxia-induced PAH in mice

To explore the role of the vasodilator DP1 and EP2 receptors in the development of PAH, we performed pulmonary hemodynamic and histological analyses in chronic hypoxia-challenged DP1^{-/-} and EP2^{-/-} mice. The DP1^{-/-} mice developed more severe PAH, with significant increases in RVSP (Supplemental Figure E4a) and in the RV/LV+S ratio (Supplemental Figure E4b) relative to WT control mice. Moreover, *DP1* deficiency enhanced hypoxia-induced pulmonary vascular remodeling in both small PAs and arterioles, as

evidenced by increased pulmonary vascular wall thickness and muscularization (Supplemental Figure E4c-h). Notably, $DP1^{-/-}$ mice had enlarged PASMCs after chronic hypoxia challenge (Supplemental Figure E4i), with increased α -SMA expression (Supplemental Figure E4j, k) and deposition of perivascular matrix proteins such as fibronectin and type I collagen (Supplemental Figure E5a-c). Similarly, the exaggerated PAH was induced in VSMC-specific deficient mice ($DP1^{F/F}SM22^{Cre}$) by hypoxia/SU5416(HySu) challenge (Figure 2a-2j). $DP1^{-/-}$ mPASMCs were larger and had higher protein/DNA ratios than control cells in response to hypoxia (Supplemental Figure E6a-c). Treatment with the DP1 inhibitor BWA868C promoted hypoxia-induced hypertrophy in hPASMCs (Supplemental E6d-f). We also observed enhanced proliferation of cultured $DP1^{-/-}$ mPASMCs and DP1 inhibitor-treated hPASMCs under hypoxic conditions (Supplemental E6g, h), but failed to detect significant increases of PCNA⁺ SMA⁺ cells in the PAs from chronic hypoxia-treated $DP1^{-/-}$ mice compared to WT controls (Supplemental Figure E6i, j). Additionally, there were no overt differences in pulmonary infiltration of CD11b⁺ and CD68⁺ inflammatory cells into perivascular areas between $DP1^{-/-}$ and WT mice after chronic hypoxia challenge (Supplemental Figure E7a, b). However, *EP2* deficiency had no significant influences on hypoxia-induced PAH and PA remodeling in mice (Supplemental Figure E8a-d).

Re-expression of DP1 in lungs attenuates PAH exacerbation induced by hypoxia in $DP1^{-/-}$ mice

Infection with DP1-expressing lentivirus via the trachea restored DP1 expression in PAs of

DP1^{-/-} mice (Supplemental Figure E9a, b). As predicted, re-introduction of DP1 attenuated hypoxia-induced pulmonary hypertension in DP1^{-/-} mice, as indicated by the decreased RVSP and RV/LV+S (Supplemental Figure E9c, d) and suppression of pulmonary vascular remodeling through a reduction in wall thickness and muscularization (Supplemental Figure E9e–g). Importantly, forced expression of DP1 also suppressed the enhancement of PASMC hypertrophy in DP1^{-/-} mice with PAH (Supplemental Figure E9h).

Pharmacological activation of DP1 inhibits progression of MCT-induced PAH and PA remodeling in rats

We next examined the therapeutic effects of the DP1-specific agonist BW245C on PAH and pulmonary vascular remodeling in MCT-treated rats. BW245C (50 µg/kg, twice a day) was administered to the rats twice daily starting from the beginning of the third week after MCT treatment (Figure 3a). MCT challenge markedly increased PA pressure in rats starting from week 2(10). Notably, BW245C administration significantly attenuated the increases in RVSP, RV/LV+S ratio, and pulmonary vascular wall thickness in MCT-treated rats (Figure 3b–f) and reversed PASMC hypertrophy and proliferation in PAs (Figure 3g–i).

DP1 deficiency promotes hypoxia-induced PASMC proliferation and hypertrophy by increasing mTORC1 activity in a PKA-dependent manner

Chronic hypoxia activates multiple proliferative signaling in VSMCs including mitogen-activated protein kinase (MAPK) and mTOR pathways(21). *DP1* deficiency had no effect on MAPK activation in cultured PASMCs under hypoxic and normoxic conditions, as determined by evaluating ERK1/2, JNK, and p38 protein phosphorylation levels

(Supplemental Figure E10). In contrast, mTORC1—a key regulator of protein synthesis in response to growth factors and nutrients—was activated in hypoxia-treated DP1^{-/-} PSMCs—as evidenced by increased phosphorylation of mTOR and its downstream target S6K (Figure 4a, b)—as well as in the lungs and PAs of chronic hypoxia-challenged DP1^{-/-} mice relative to their WT counterparts (Supplemental Figure E11a, b). However, *DPI* deficiency had no effect on mTORC2 activity in PSMCs, as determined by AKT phosphorylation at Ser473 (Supplemental Figure E12). Forced expression of DP1 (Figure 4c) attenuated the increase in mTORC1 activity in hypoxia-treated DP1^{-/-} PSMCs (Figure 4c, d).

mTORC1 is composed of mTOR, raptor, and GβL as well as the inhibitory PRAS40. A well-established upstream regulator of mTORC1 is the phosphoinositide 3-kinase (PI3K)/AKT signaling pathway that phosphorylates PRAS40 or tuberous sclerosis complex, another negative regulator of mTORC1(22). Unexpectedly, we did not observe an increase in AKT activity or PRAS40 phosphorylation in DP1^{-/-} mPSMCs under hypoxic and normoxic conditions as compared to WT mPSMCs (Supplemental Figure E13a). Accordingly, PI3K inhibition failed to reverse the hypoxia-induced reduction in mTORC1 activity in DP1-overexpressing mPSMCs (Supplemental Figure E13b). Like AKT, AMPK directly communicates with mTORC1 through phosphorylation of raptor, leading to the allosteric inhibition of the complex(23). However, we did not detect any changes in AMPK activity or raptor phosphorylation at Ser792 in DP1^{-/-} mPSMCs (Supplemental Figure E14a,b).

DP1 is connected to the cAMP signaling cascade through Gαs protein(24). *DPI*

deletion reduced cAMP production in mPASCs in response to DP1 agonist treatment (Figure 4e). cAMP/PKA signaling has been shown to suppress mTOR activity(25, 26). We also found that PKA inhibition restored mTORC1 activity in DP1 re-expressing DP1^{-/-} mPASCs in response to hypoxia (Figure 4f).

Inhibition of mTOR alleviates PAH exacerbation induced by hypoxia in DP1^{-/-} mice

Treatment with the mTOR inhibitor rapamycin abolished the increases in proliferation and hypertrophy (Supplemental Figure E15a, b), and the enhancing cell traction force (Supplemental Figure E15c, d) in cultured DP1^{-/-} mPASCs under hypoxia. Additionally, rapamycin reduced the degree of pulmonary hypertension (Figure 5a, b), PA remodeling (Figure 5c–f), and PASC hypertrophy in chronic hypoxia-challenged DP1^{-/-} mice (Figure 5g–i).

DP1 deficiency enhances mTORC1 activity in mPASCs via PKA-mediated mTORC1 dissociation

The integrity of the mTOR complex is essential for its kinase activity and signal transduction(27). To investigate whether *DP1* deficiency enhances mTORC1 activity by influencing the association of mTOR with raptor and PRAS40, mTOR was immunoprecipitated from hypoxia-treated mPASCs and the blot was probed with antibodies against mTOR, raptor, PRAS40, and GβL. *DP1* deficiency enhanced the binding of raptor to mTOR in mPASCs in response to hypoxia, which was accompanied by increased mTOR activity and S6K phosphorylation (Figure 6a). Re-introducing DP1 into these cells abolished mTORC1 activation by inducing its dissociation from raptor, although

mTORC1 activity was restored by PKA inhibition (Figure 6b, c). Since raptor phosphorylation status determines mTORC1 activity(28, 29), we investigated whether raptor itself is a target of PKA. By aligning the raptor protein amino acid sequences of different species, we identified a conserved RRXS motif for PKA phosphorylation at Ser791 (Figure 6d). The *in vitro* kinase activity assay showed that the S791A raptor mutant was not phosphorylated by PKA (Figure 6e). Moreover, forskolin induced the phosphorylation of the PKA substrate motif in myc-tagged WT raptor but not the S791A mutant in transfected mPASCs (Figure 6f). To further confirm PKA-mediated raptor phosphorylation, we developed an antibody that specifically recognizes the phosphorylated Ser791 site of raptor (Supplemental Figure E16). DP1 agonist treatment enhanced raptor Ser791 phosphorylation and suppressed mTORC1 activity, whereas DP1 antagonist had the opposite effects (Figure 6g). The phosphorylation of raptor Ser791 in mPASCs induced by DP1 agonist was associated with decreased binding to mTOR, these effects were abolished by expression of S791A-mutant raptor (Figure 6h). Collectively, DP1 activation represses mTORC1 activity by promoting its complex dissociation through PKA-dependent Ser791 phosphorylation of raptor in PASCs exposed to hypoxia (Figure 6i).

Treprostinil ameliorates HySU-induced PAH in mice by activating both IP and DP1

We then investigated whether treprostinil suppresses PAH development in part through activation of DP1. After 3 weeks of exposure to hypoxic conditions (10% O₂) and SU5416 administration, IP^{-/-}, DP1^{-/-}, and double-mutant (IP^{-/-}DP1^{-/-}) mice developed more severe PAH (Figure 7a, b) with aggravated PA remodeling, as evidenced by increased pulmonary

vascular wall thickness and muscularization relative to control mice (Figure 7c–f). Treprostinil treatment reversed the exacerbation of pulmonary hypertension and PA remodeling induced by HySU in $IP^{-/-}$ and $DP1^{-/-}$ mutants but not in $IP^{-/-}DP1^{-/-}$ mice (Figure 7). Indeed, treprostinil inhibited mTORC1 activity and downstream S6K phosphorylation in human PSMCs (Supplemental Figure E17a) as well as PAs from HySU-challenged mice (Supplemental Figure E17b). Thus, treprostinil prevents the progression of PAH at least in part through activation of DP1 receptor.

Discussion

DP1 receptor mediates vasodilation of human arteries including PAs(12, 30). In the present study, we found that DP1 was downregulated in PAs in rodent models of PAH and idiopathic patients. *DP1* deficiency exacerbated hypoxia-induced PAH and enhanced PA remodeling in mice through activation of mTORC1 signaling. We determined that DP1 activation promoted mTORC1 complex dissociation and suppressed mTORC1 activity in PSMCs through PKA-mediated raptor phosphorylation. Thus, DP1 activation confers protection against hypoxia-induced PAH through PKA/raptor-dependent mTORC1 dissociation.

Increased contractility of small PAs and arterioles is a pathological feature of pulmonary hypertension. This is associated with heightened secretion of vasoconstrictor substances such as Tx and endothelin-1 and inhibition of vasodilator PGI_2 and nitric oxide release in PAH patients(31-33). DP1 plays an important role in maintaining blood flow and hemostasis in rodents and humans, including brain blood flow after ischemia–reperfusion injury and nicotinic acid-induced vasodilation(30, 34). Despite the elevation in PGD_2

production in patients with primary PAH(35), we and others(11) have observed downregulation of DP1 in PAs in PAH rodent models. *DP1* deficiency intensified hypoxia-induced PAH and PA remodeling in mice, while DP1 agonist inhibited PAH progression in mice. Additionally, infusion of large amounts of PGD₂ reversed pulmonary hypertension in newborn lambs(36). These results imply that decreased DP1 expression in PAs contributes to the pathogenesis of PAH.

mTOR is a member of the serine/threonine protein kinase family that regulates cell proliferation, protein synthesis, cell motility, gene transcription, and autophagy, and it also is the central component of mTORC1 and mTORC2. The two complexes are localized in different cellular organelles and have distinct functions(37): mTORC1 regulates protein synthesis and acts as a cellular nutrient, energy, and redox sensor, whereas mTORC2 regulates the actin cytoskeleton and cellular metabolism. PASMC proliferation and hypertrophy are major contributors to pulmonary vascular remodeling in PAH. The mTORC1 and mTORC2 pathways are both activated in PAs and isolated distal PASMCs from patients with idiopathic PAH, and are required for PASMCs proliferation induced by chronic hypoxia in vivo and in vitro(38). Pharmacological inhibition of mTOR kinases attenuates hypoxia-induced PA remodeling and right ventricular hypertrophy in rodents(39) and can improve PAH in patients(40). We found that *DP1* deficiency promoted PASMC proliferation and hypertrophy under hypoxic conditions and in pulmonary vessels of MCT-treated rats. However, we did not detect significant increases in PASMC proliferation in hypoxia-treated *DP1*^{-/-} mice, likely due to the less severe pulmonary response induced by chronic hypoxia in mouse models(41). In agreement with the findings in *DP1*^{-/-} mice, enhanced PASMC

hypertrophy has also been reported in hypoxia-exposed *COX-2*-deficient mice(3). Interestingly, *DPI* deletion stimulated mTORC1 activity in hypoxia-treated mPASCs without affecting that of mTORC2, while rapamycin treatment abolished the enhancement of PAMSC hypertrophy and proliferation in *DPI*-deficient PASCs, indicating that DP1 activation may alleviate hypoxia-induced PAH via suppression of mTORC1 signaling. However, DP1 expression and its downstream mTORC1 signaling alterations in treprostinil-treated PAH patients warrants further investigation.

Raptor interacting with mTOR functions as a scaffold protein that facilitates the recruitment of substrates such as S6K1 and 4EBP1 to mTORC1(42). The integrity of mTOR complexes is critical for mTOR activity, and dissociation of raptor and mTOR protein suppresses the intrinsic catalytic activity of mTORC1(26, 43). A three-dimensional structural analysis has shown that rapamycin inhibits mTORC1 by inducing the dissociation of raptor from mTOR complex(27). On the contrary, dissociation of the inhibitory component PRAS40 from the complex induced by AKT/PKB-mediated phosphorylation leads to induction of mTORC1 activity(44). We found that DP1 activation suppressed hypoxia-induced activation of mTORC1 by promoting raptor dissociation from mTOR in PASCs. DP1 is coupled to $G_{\alpha s}$ and its activation leads to an increase in intracellular cAMP production. *DPI* deficiency caused a marked reduction in intracellular cAMP levels and consequently, PKA activity in hypoxia-exposed PASCs. Raptor phosphorylation is critical for mTORC1 activation and multiple phosphorylation sites have been identified in raptor protein(28). For instance, raptor phosphorylation at Ser722/Ser792 is required for AMPK-mediated inhibition of mTORC1 activity(23). By mutagenesis experiments and using a phosphorylation-specific antibody, we

and others(45) identified a conserved PKA phosphorylation site (Ser791) in raptor protein and showed that DP1 agonist treatment increased cellular cAMP generation and Ser791 phosphorylation in raptor, which promoted raptor dissociation from mTORC1. Mutation of Ser791 to Ala suppressed DP1 activation-induced dissociation of raptor from mTORC1 and reduced complex activity in PSMCs. In accordance with our findings, cAMP/PKA-dependent dissociation of mTORC1 and inhibition of mTORC1 has been observed in embryonic fibroblasts and HEK293 cells(25, 26), 3T3-L1 adipocytes(46), and lung fibroblasts(47). However, under some circumstances, PKA-driven mTORC1 activation is reported in mediation of the biological activities of hormones—e.g., catecholamine-stimulated adipose browning(45) and thyroid-stimulating hormone-induced proliferation(48). In fact, the regulatory subunit of PKA (PRKAR1A) physically interacts with mTOR kinase and influences its auto-phosphorylation and activity(49), while the catalytic subunit of PKA directly phosphorylates mTOR kinase at different sites(45) and regulates mTOR substrates(50), thereby increasing the complexity of crosstalk between PKA and mTORC1. Thus, regulation of mTORC1 signaling by cAMP/PKA varies depending on cell type and biological context.

In summary, DP1 activation slows the progression of PAH in rodents by PKA-mediated suppression of mTORC1 activity. Thus, targeting the DP1/PKA/mTORC1 pathway may represent a promising therapeutic strategy for the treatment of PAH.

Disclosures

None.

References

1. Rabinovitch M. Molecular pathogenesis of pulmonary arterial hypertension. *J Clin Invest* 2012; 122: 4306-4313.
2. Pullamsetti SS, Schermuly R, Ghofrani A, Weissmann N, Grimminger F, Seeger W. Novel and emerging therapies for pulmonary hypertension. *Am J Respir Crit Care Med* 2014; 189: 394-400.
3. Fredenburgh LE, Liang OD, Macias AA, Polte TR, Liu X, Riascos DF, Chung SW, Schissel SL, Ingber DE, Mitsialis SA, Kourembanas S, Perrella MA. Absence of cyclooxygenase-2 exacerbates hypoxia-induced pulmonary hypertension and enhances contractility of vascular smooth muscle cells. *Circulation* 2008; 117: 2114-2122.
4. El Yafawi R, Wirth JA. What Is the Role of Oral Prostacyclin Pathway Medications in Pulmonary Arterial Hypertension Management? *Curr Hypertens Rep* 2017; 19: 97.
5. Kuwano K, Hashino A, Asaki T, Hamamoto T, Yamada T, Okubo K, Kuwabara K. 2-[4-[(5,6-diphenylpyrazin-2-yl)(isopropyl)amino]butoxy]-N-(methylsulfonyl)acetamide (NS-304), an orally available and long-acting prostacyclin receptor agonist prodrug. *J Pharmacol Exp Ther* 2007; 322: 1181-1188.
6. Voswinckel R, Enke B, Reichenberger F, Kohstall M, Kreckel A, Krick S, Gall H, Gessler T, Schmehl T, Ghofrani HA, Schermuly RT, Grimminger F, Rubin LJ, Seeger W, Olschewski

- H. Favorable effects of inhaled treprostinil in severe pulmonary hypertension: results from randomized controlled pilot studies. *J Am Coll Cardiol* 2006; 48: 1672-1681.
7. Chen H, Rosenzweig EB, Gotzkowsky SK, Arneson C, Nelsen AC, Bourge RC. Treatment satisfaction is associated with improved quality of life in patients treated with inhaled treprostinil for pulmonary arterial hypertension. *Health Qual Life Outcomes* 2013; 11: 31.
8. Abramovitz M, Adam M, Boie Y, Carriere M, Denis D, Godbout C, Lamontagne S, Rochette C, Sawyer N, Tremblay NM, Belley M, Gallant M, Dufresne C, Gareau Y, Ruel R, Juteau H, Labelle M, Ouimet N, Metters KM. The utilization of recombinant prostanoid receptors to determine the affinities and selectivities of prostaglandins and related analogs. *Biochim Biophys Acta* 2000; 1483: 285-293.
9. Whittle BJ, Silverstein AM, Mottola DM, Clapp LH. Binding and activity of the prostacyclin receptor (IP) agonists, treprostinil and iloprost, at human prostanoid receptors: treprostinil is a potent DP1 and EP2 agonist. *Biochem Pharmacol* 2012; 84: 68-75.
10. Lu A, Zuo C, He Y, Chen G, Piao L, Zhang J, Xiao B, Shen Y, Tang J, Kong D, Alberti S, Chen D, Zuo S, Zhang Q, Yan S, Fei X, Yuan F, Zhou B, Duan S, Yu Y, Lazarus M, Su Y, Breyer RM, Funk CD. EP3 receptor deficiency attenuates pulmonary hypertension through suppression of Rho/TGF-beta1 signaling. *J Clin Invest* 2015; 125: 1228-1242.
11. Morrison K, Studer R, Ernst R, Haag F, Kauser K, Clozel M. Differential effects of Selexipag [corrected] and prostacyclin analogs in rat pulmonary artery. *J Pharmacol Exp Ther* 2012; 343: 547-555.

12. Walch L, Labat C, Gascard JP, de Montpreville V, Brink C, Norel X. Prostanoid receptors involved in the relaxation of human pulmonary vessels. *Br J Pharmacol* 1999; 126: 859-866.
13. Patel JA, Shen L, Hall SM, Benyahia C, Norel X, McAnulty RJ, Moledina S, Silverstein AM, Whittle BJ, Clapp LH. Prostanoid EP(2) Receptors Are Up-Regulated in Human Pulmonary Arterial Hypertension: A Key Anti-Proliferative Target for Treprostinil in Smooth Muscle Cells. *Int J Mol Sci* 2018; 19.
14. Benyahia C, Boukais K, Gomez I, Silverstein A, Clapp L, Fabre A, Danel C, Leseche G, Longrois D, Norel X. A comparative study of PGI₂ mimetics used clinically on the vasorelaxation of human pulmonary arteries and veins, role of the DP-receptor. *Prostaglandins Other Lipid Mediat* 2013; 107: 48-55.
15. Kong D, Shen Y, Liu G, Zuo S, Ji Y, Lu A, Nakamura M, Lazarus M, Stratakis CA, Breyer RM, Yu Y. PKA regulatory I α subunit is essential for PGD₂-mediated resolution of inflammation. *J Exp Med* 2016; 213: 2209-2226.
16. DuPage M, Dooley AL, Jacks T. Conditional mouse lung cancer models using adenoviral or lentiviral delivery of Cre recombinase. *Nat Protoc* 2009; 4: 1064-1072.
17. Paddenbergh R, Stieger P, von Lilien AL, Faulhammer P, Goldenberg A, Tillmanns HH, Kummer W, Braun-Dullaeus RC. Rapamycin attenuates hypoxia-induced pulmonary vascular remodeling and right ventricular hypertrophy in mice. *Respir Res* 2007; 8: 15.
18. Kovacs L, Cao Y, Han W, Meadows L, Kovacs-Kasa A, Kondrikov D, Verin AD, Barman SA, Dong Z, Huo Y, Su Y. PFKFB3 in Smooth Muscle Promotes Vascular Remodeling in

Pulmonary Arterial Hypertension. *Am J Respir Crit Care Med* 2019; 200: 617-627.

19. Nikam VS, Schermuly RT, Dumitrascu R, Weissmann N, Kwapiszewska G, Morrell N, Klepetko W, Fink L, Seeger W, Voswinckel R. Treprostinil inhibits the recruitment of bone marrow-derived circulating fibrocytes in chronic hypoxic pulmonary hypertension. *Eur Respir J* 2010; 36: 1302-1314.
20. Loukanov T, Jaschinski C, Kirilov M, Klimpel H, Karck M, Gorenflo M. Cyclooxygenase-2 expression in lung in patients with congenital heart malformations and pulmonary arterial hypertension. *Thorac Cardiovasc Surg* 2013; 61: 307-311.
21. Stenmark KR, Fagan KA, Frid MG. Hypoxia-induced pulmonary vascular remodeling: cellular and molecular mechanisms. *Circ Res* 2006; 99: 675-691.
22. LoPiccolo J, Blumenthal GM, Bernstein WB, Dennis PA. Targeting the PI3K/Akt/mTOR pathway: effective combinations and clinical considerations. *Drug Resist Updat* 2008; 11: 32-50.
23. Gwinn DM, Shackelford DB, Egan DF, Mihaylova MM, Mery A, Vasquez DS, Turk BE, Shaw RJ. AMPK phosphorylation of raptor mediates a metabolic checkpoint. *Mol Cell* 2008; 30: 214-226.
24. Hata AN, Breyer RM. Pharmacology and signaling of prostaglandin receptors: multiple roles in inflammation and immune modulation. *Pharmacol Ther* 2004; 103: 147-166.
25. Mavrakis M, Lippincott-Schwartz J, Stratakis CA, Bossis I. Depletion of type IA regulatory

- subunit (RI α) of protein kinase A (PKA) in mammalian cells and tissues activates mTOR and causes autophagic deficiency. *Hum Mol Genet* 2006; 15: 2962-2971.
26. Xie J, Ponuwei GA, Moore CE, Willars GB, Tee AR, Herbert TP. cAMP inhibits mammalian target of rapamycin complex-1 and -2 (mTORC1 and 2) by promoting complex dissociation and inhibiting mTOR kinase activity. *Cell Signal* 2011; 23: 1927-1935.
27. Yip CK, Murata K, Walz T, Sabatini DM, Kang SA. Structure of the human mTOR complex I and its implications for rapamycin inhibition. *Mol Cell* 2010; 38: 768-774.
28. Foster KG, Acosta-Jaquez HA, Romeo Y, Ekim B, Soliman GA, Carriere A, Roux PP, Ballif BA, Fingar DC. Regulation of mTOR complex 1 (mTORC1) by raptor Ser863 and multisite phosphorylation. *J Biol Chem* 2010; 285: 80-94.
29. Wu XN, Wang XK, Wu SQ, Lu J, Zheng M, Wang YH, Zhou H, Zhang H, Han J. Phosphorylation of Raptor by p38 β participates in arsenite-induced mammalian target of rapamycin complex 1 (mTORC1) activation. *J Biol Chem* 2011; 286: 31501-31511.
30. Cheng K, Wu TJ, Wu KK, Sturino C, Metters K, Gottesdiener K, Wright SD, Wang Z, O'Neill G, Lai E, Waters MG. Antagonism of the prostaglandin D2 receptor 1 suppresses nicotinic acid-induced vasodilation in mice and humans. *Proc Natl Acad Sci U S A* 2006; 103: 6682-6687.
31. Christman BW, McPherson CD, Newman JH, King GA, Bernard GR, Groves BM, Loyd JE. An imbalance between the excretion of thromboxane and prostacyclin metabolites in pulmonary hypertension. *N Engl J Med* 1992; 327: 70-75.

32. Giaid A, Saleh D. Reduced expression of endothelial nitric oxide synthase in the lungs of patients with pulmonary hypertension. *N Engl J Med* 1995; 333: 214-221.
33. Giaid A, Yanagisawa M, Langleben D, Michel RP, Levy R, Shennib H, Kimura S, Masaki T, Duguid WP, Stewart DJ. Expression of endothelin-1 in the lungs of patients with pulmonary hypertension. *N Engl J Med* 1993; 328: 1732-1739.
34. Ahmad AS. PGD2 DP1 receptor stimulation following stroke ameliorates cerebral blood flow and outcomes. *Neuroscience* 2014; 279: 260-268.
35. Robbins IM, Barst RJ, Rubin LJ, Gaine SP, Price PV, Morrow JD, Christman BW. Increased levels of prostaglandin D(2) suggest macrophage activation in patients with primary pulmonary hypertension. *Chest* 2001; 120: 1639-1644.
36. Soifer SJ, Morin FC, 3rd, Heymann MA. Prostaglandin D2 reverses induced pulmonary hypertension in the newborn lamb. *J Pediatr* 1982; 100: 458-463.
37. Betz C, Hall MN. Where is mTOR and what is it doing there? *J Cell Biol* 2013; 203: 563-574.
38. Goncharov DA, Kudryashova TV, Ziai H, Ihida-Stansbury K, DeLisser H, Krymskaya VP, Tuder RM, Kawut SM, Goncharova EA. Mammalian target of rapamycin complex 2 (mTORC2) coordinates pulmonary artery smooth muscle cell metabolism, proliferation, and survival in pulmonary arterial hypertension. *Circulation* 2014; 129: 864-874.
39. Pena A, Kobir A, Goncharov D, Goda A, Kudryashova TV, Ray A, Vanderpool R, Baust J, Chang B, Mora AL, Gorcsan J, 3rd, Goncharova EA. Pharmacological Inhibition of mTOR Kinase

- Reverses Right Ventricle Remodeling and Improves Right Ventricle Structure and Function in Rats. *Am J Respir Cell Mol Biol* 2017; 57: 615-625.
40. Wessler JD, Steingart RM, Schwartz GK, Harvey BG, Schaffer W. Dramatic improvement in pulmonary hypertension with rapamycin. *Chest* 2010; 138: 991-993.
41. Sztuka K, Jasinska-Stroschein M. Animal models of pulmonary arterial hypertension: A systematic review and meta-analysis of data from 6126 animals. *Pharmacol Res* 2017; 125: 201-214.
42. Kim DH, Sarbassov DD, Ali SM, King JE, Latek RR, Erdjument-Bromage H, Tempst P, Sabatini DM. mTOR interacts with raptor to form a nutrient-sensitive complex that signals to the cell growth machinery. *Cell* 2002; 110: 163-175.
43. Oshiro N, Yoshino K, Hidayat S, Tokunaga C, Hara K, Eguchi S, Avruch J, Yonezawa K. Dissociation of raptor from mTOR is a mechanism of rapamycin-induced inhibition of mTOR function. *Genes Cells* 2004; 9: 359-366.
44. Vander Haar E, Lee SI, Bandhakavi S, Griffin TJ, Kim DH. Insulin signalling to mTOR mediated by the Akt/PKB substrate PRAS40. *Nat Cell Biol* 2007; 9: 316-323.
45. Liu D, Bordicchia M, Zhang C, Fang H, Wei W, Li JL, Guilherme A, Guntur K, Czech MP, Collins S. Activation of mTORC1 is essential for beta-adrenergic stimulation of adipose browning. *J Clin Invest* 2016; 126: 1704-1716.
46. Scott PH, Lawrence JC, Jr. Attenuation of mammalian target of rapamycin activity by increased

- cAMP in 3T3-L1 adipocytes. *J Biol Chem* 1998; 273: 34496-34501.
47. Okunishi K, DeGraaf AJ, Zaslona Z, Peters-Golden M. Inhibition of protein translation as a novel mechanism for prostaglandin E2 regulation of cell functions. *FASEB J* 2014; 28: 56-66.
48. Blancquaert S, Wang L, Paternot S, Coulonval K, Dumont JE, Harris TE, Roger PP. cAMP-dependent activation of mammalian target of rapamycin (mTOR) in thyroid cells. Implication in mitogenesis and activation of CDK4. *Mol Endocrinol* 2010; 24: 1453-1468.
49. Mavrakis M, Lippincott-Schwartz J, Stratakis CA, Bossis I. mTOR kinase and the regulatory subunit of protein kinase A (PRKAR1A) spatially and functionally interact during autophagosome maturation. *Autophagy* 2007; 3: 151-153.
50. Lecureuil C, Tesseraud S, Kara E, Martinat N, Sow A, Fontaine I, Gauthier C, Reiter E, Guillou F, Crepieux P. Follicle-stimulating hormone activates p70 ribosomal protein S6 kinase by protein kinase A-mediated dephosphorylation of Thr 421/Ser 424 in primary Sertoli cells. *Mol Endocrinol* 2005; 19: 1812-1820.

Figure Legends

Figure 1. DP1 is downregulated in PASMCs in response to hypoxia. (a) Relative mRNA levels of DP1/2 in lung PAs from mice subjected to chronic hypoxia. *P < 0.05 vs. normoxia (n = 7–10). (b) Relative mRNA levels of DP1/2 in lung PAs from MCT-treated rats. *P < 0.05 vs. control (n = 5–7). (c) Relative mRNA levels of DP1/2 in cultured mPASMCs in response to hypoxia. *P < 0.05 vs. control (n = 5). (d) Relative mRNA levels of DP1/2 in cultured hPASMCs in response to hypoxia. *P < 0.05 vs. control (n = 5-6). (e) Representative immunofluorescence images of DP1 (red) and α -SMA (green) expression in lung tissue from hypoxia-treated mice. Scale bar: 25 μ m. (f) Quantification of DP1 expression in panel E. *P < 0.05 vs. normal (n = 7). (g) Representative immunofluorescence images of DP1 (red) and α -SMA (green) expression in lung tissue from PAH patients. Scale bar: 25 μ m. (h) Quantification of DP1 expression in panel F. *P < 0.05 vs. normal (n = 7). Data represent mean \pm SEM. Statistical significance was evaluated with the two-tailed Student's t test.

Figure 2. VSMC-specific DP1 deletion aggravates hypoxia-induced PAH and PA remodeling in mice. (a) Genotyping of VSMC-specific DP1 knockout mice by PCR of genomic DNA extracted from tail biopsies. (b) RVSP in DP1^{F/F}SM22^{Cre} and DP1^{F/F} mice after hypoxia/SU5416 (HySu) treatment. *P < 0.05 vs. DP1^{F/F}; #P < 0.05 vs. control (n = 7-9). (c) RV/LV+S in DP1^{F/F}SM22^{Cre} and DP1^{F/F} mice after HySu treatment. *P < 0.05 vs. DP1^{F/F}; #P < 0.05 vs. control (n = 7-9). (d, e) Representative hematoxylin and eosin-stained sections of small PAs and arterioles from HySu-treated DP1^{F/F}SM22^{Cre} and DP1^{F/F} mice. Scale bars: 50 and 25 μ m, respectively. (f) Representative immunofluorescence images of α -SMA (green)

expression in small PAs (d) and arterioles (e) from HySu-treated DP1^{F/F}SM22^{Cre} and DP1^{F/F} mice. Scale bars: 50 and 25 μm , respectively. (g) Quantification of the ratio of vascular medial thickness to total vessel size for the HySu treatment model. *P < 0.05 vs. DP1^{F/F}; #P < 0.05 vs. control (n = 8 or 9). (h) Proportion of partially and fully muscularized PAs (diameter: 20–50 μm) from HySu-treated mice. *P < 0.05 vs. DP1^{F/F}; #P < 0.05 vs. control (n = 8 or 9). (i) Quantification of PASMC size in PAs from HySu-treated DP1^{F/F}SM22^{Cre} and DP1^{F/F} mice. *P < 0.05 vs. DP1^{F/F}; #P < 0.05 vs. control (n = 8 or 9). Data represent mean \pm SEM. Statistical significance was evaluated by two-way analysis of variance with Bonferroni post-hoc analysis.

Figure 3. DP1 agonist treatment suppresses progression of MCT-induced PAH in rats.

(a) Protocol for administration of DP1 agonist BW245C to rats after MCT challenge. (b, c) Effect of BW245C administration on RVSP and RV/LV+S ratio in MCT-treated rats. *P < 0.05 vs. PBS; #P < 0.05 vs. vehicle (n = 6–8). (d) Representative hematoxylin and eosin-stained lung sections of MCT-injected rats treated with BW245C. Scale bar: 50 μm . (e) Representative immunofluorescence images of α -SMA (green) expression in lung sections of MCT-injected rats treated with BW245C. Scale bar: 25 μm , (f) Quantification of the ratio of vascular medial thickness to total vessel size in MCT-challenged rats after BW245C treatment. *P < 0.05 vs. PBS; #P < 0.05 vs. vehicle (n = 6–8). (g) Quantification of PASMC size in PAs of MCT- challenged rats after BW245C treatment. *P < 0.05 vs. PBS; #P < 0.05 vs. vehicle (n = 6–8). (h) Representative immunofluorescence images of α -SMA (green) and PCNA (red) expression in lung sections of MCT-challenged rats after BW245C treatment. Scale bar: 25 μm , (i) Quantification of PCNA-positive cells in H. *P < 0.05 vs. PBS; #P <

0.05 vs. vehicle (n = 6–8). Data represent mean \pm SEM. Statistical significance was evaluated by two-way analysis of variance with Bonferroni post-hoc analysis.

Figure 4. DP1 deficiency enhances mTOR activity in PSMCs in response to hypoxia via cAMP/PKA signaling. (a) Expression levels of mTOR signaling components in cultured mPSMCs under normoxia or hypoxia, as determined by western blotting. (b) Quantification of p-mTOR and p-S6K protein levels in panel A. *P < 0.05 vs. WT; #P < 0.05 vs. normoxia (n = 4). (c) Expression levels of mTOR signaling components in cultured DP1^{-/-} mPSMCs with DP1 re-expression under normoxia or hypoxia, as determined by western blotting. (d) Quantification of p-mTOR and p-S6K protein levels in panel C. *P < 0.05 vs. WT; #P < 0.05 vs. normoxia (n = 4). (e) Effect of DP1 agonist BW245C treatment on intracellular cAMP levels in WT and DP1^{-/-} mPSMCs. *P < 0.05 vs. WT (n = 4–6). (f) Effect of PKA inhibitor H-89 treatment (10 μ mol/l) on mTOR signaling in cultured mPSMCs re-expressing DP1 under normoxia or hypoxia. Data represent mean \pm SEM. Statistical significance was evaluated by two-way analysis of variance with Bonferroni post-hoc analysis.

Figure 5. mTOR inhibition attenuates PAH exacerbation in hypoxia-exposed DP1^{-/-} mice. (a, b) Effect of rapamycin on RVSP and RV/LV+S ratio of hypoxia-treated mice. *P < 0.05 vs. WT; #P < 0.05 vs. control (n = 8 or 9). (c, d) Representative hematoxylin and eosin-stained sections of small PAs and arterioles from hypoxia-challenged DP1^{-/-} and WT mice after rapamycin treatment. (e) Quantification of the ratio of vascular medial thickness to total vessel size in hypoxia-challenged mice after rapamycin treatment. *P < 0.05 vs. WT; #P < 0.05 vs. control (n = 7–9). (f) Proportion of partially and fully muscularized pulmonary

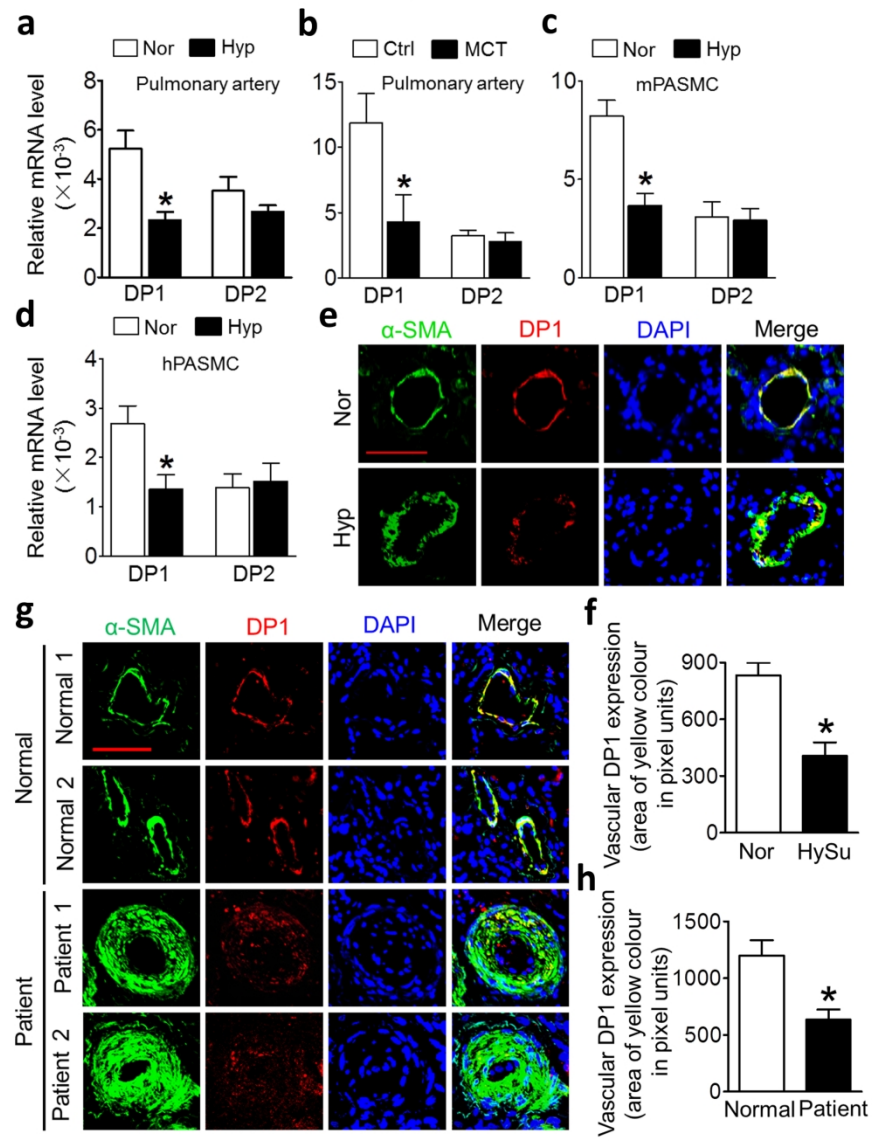
arterioles (20–50 μm in diameter) in hypoxia-exposed mice following rapamycin treatment. * $P < 0.05$ vs. WT; # $P < 0.05$ vs. control (n = 8 or 9). (g) Quantification of PASMC size in PAs from hypoxia-challenged mice after rapamycin treatment. * $P < 0.05$ vs. WT; # $P < 0.05$ vs. control (n = 8 or 9). (h) Representative immunofluorescence images of α -SMA (green) and PCNA (red) expression in lung sections of hypoxia-challenged mice after rapamycin treatment. Scale bar: 25 μm . (i) Quantification of PCNA-positive cells in panel H. * $P < 0.05$ vs. WT; # $P < 0.05$ vs. control (n = 6 or 7). Data represent mean \pm SEM. Statistical significance was evaluated by two-way analysis of variance with Bonferroni post-hoc analysis.

Figure 6. DP1 deficiency enhances mTORC1 activity in hypoxia-treated mPASMCs via PKA-induced raptor dissociation from mTORC1. (a) Expression levels of mTORC1 and signaling components in hypoxia-treated WT and DP1^{-/-} mPASMCs, as determined by western blotting. (b) Effect of PKA inhibitor H-89 (10 $\mu\text{mol/l}$) on the association of mTORC1 components in mPASMCs re-expressing DP1. (c) Quantification of mTOR–raptor association in panel B. * $P < 0.05$ vs. indicated group (n = 3). (d) Amino acid sequence alignment of human, mouse, rat, cow, and frog raptor proteins. Ser791 is indicated by an arrowhead; box indicates p-PKA substrate motif. (e) Top panel: Autoradiogram of ³²P-labeled recombinant WT raptor (WT) and Ser791→Ala (S791A) mutant protein following incubation with PKA. Bottom panel: Coomassie Blue-stained gel of raptor used for the above phosphorylation assay. (f) Western blot analysis of p-PKA-substrate (RRXS*/T*) and raptor expression in forskolin-treated mPASMCs expressing myc-tagged WT and S791A mutant raptor. (g) Detection of p-raptor (Ser791) and mTOR signaling components in

mPASMCs following BW245C (0.5 μ M) or BWA868C (10 μ M) treatment by western blotting. (h) Western blot analysis of p-raptor (Ser791)-induced raptor dissociation from mTORC1 in mPASMCs after BW245C treatment. (i) Schematic illustration of DP1-mediated PASMC homeostasis through PKA/RAPTOR/mTORC1 signaling. Data represent mean \pm SEM. Statistical significance was evaluated by two-way analysis of variance with Bonferroni post-hoc analysis.

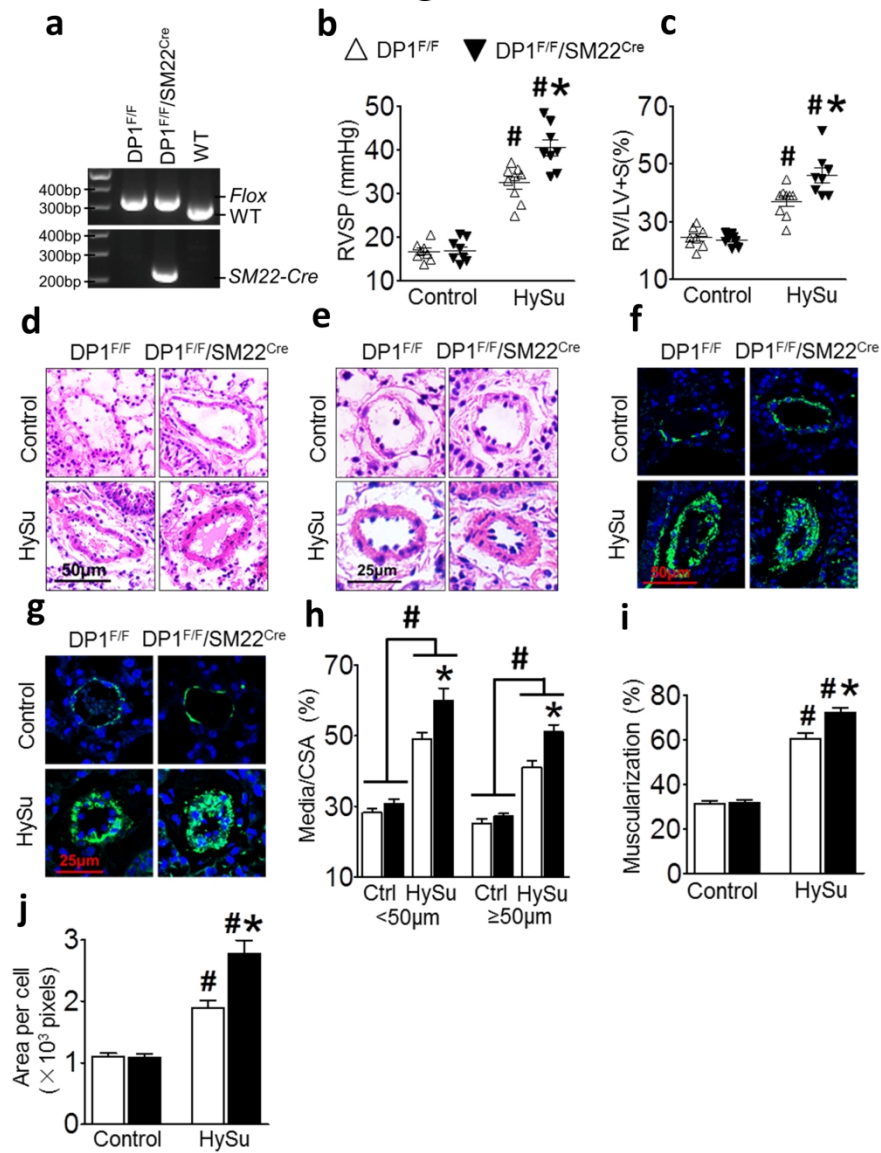
Figure 7. Treprostinil protects against HySU-induced PAH in mice via activation of DP1 and IP receptors. (a, b) RVSP and RV/LV+S ratio in HySU-challenged DP1^{-/-}, IP^{-/-}, DP^{-/-} IP^{-/-}, and WT mice with or without treprostinil treatment. *P < 0.05 vs. WT or as indicated; #P < 0.05 vs. vehicle (n = 7 or 8). (c, d) Representative hematoxylin and eosin-stained lung tissue sections and immunofluorescence images of α -SMA (green) expression in lung tissue of HySU-challenged IP^{-/-}, DP^{-/-} IP^{-/-}, and WT mice with or without treprostinil treatment. Scale bar: 25 μ m. (e) Quantification of the ratio of vascular medial thickness to total vessel size in HySU-challenged DP1^{-/-}, IP^{-/-}, DP^{-/-} IP^{-/-}, and WT mice with or without treprostinil treatment. *P < 0.05 vs. WT or as indicated; #P < 0.05 vs. vehicle (n = 7 or 8). (f) Proportion of partially and fully muscularized pulmonary arterioles (diameter: 20–50 μ m) in HySU-challenged DP1^{-/-}, IP^{-/-}, DP^{-/-} IP^{-/-}, and WT mice with or without treprostinil treatment. *P < 0.05 vs. WT or as indicated; #P < 0.05 vs. vehicle (n = 7 or 8). Data represent mean \pm SEM. Statistical significance was evaluated by two-way analysis of variance with Bonferroni post-hoc analysis.

Figure 1



190x253mm (300 x 300 DPI)

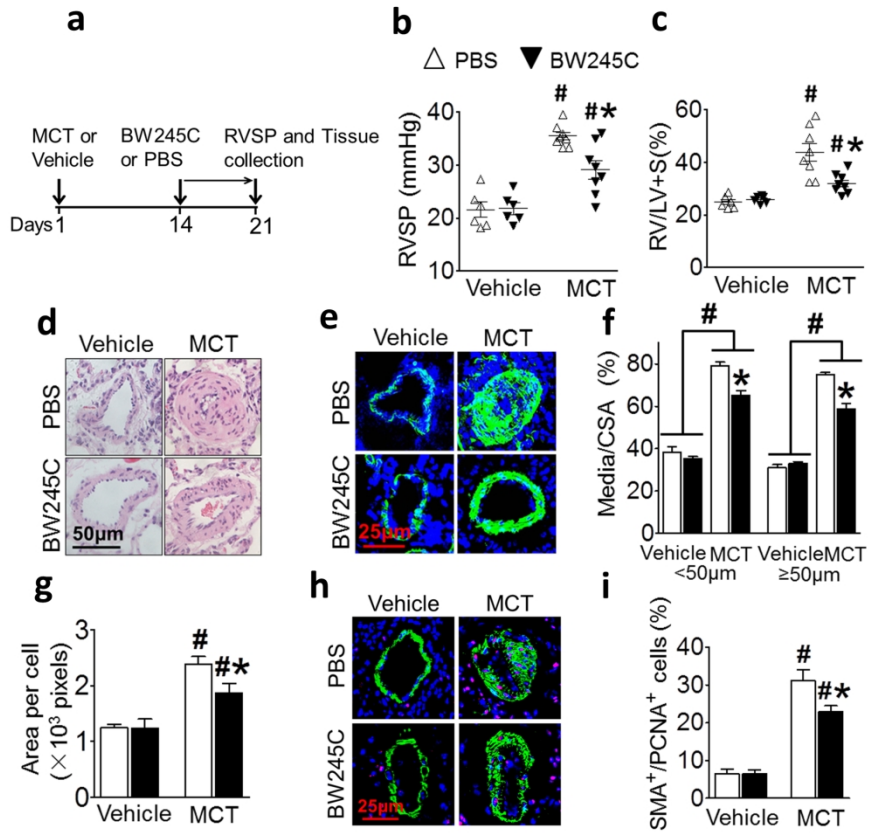
Figure 2



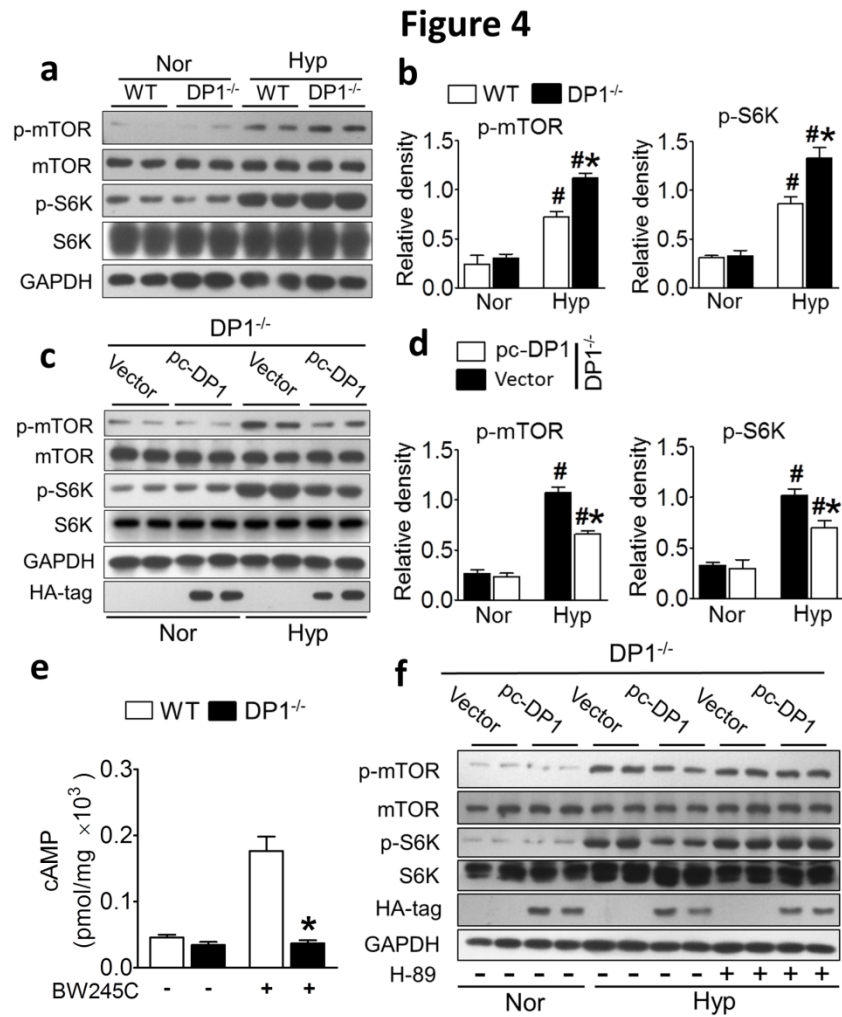
F2

190x253mm (300 x 300 DPI)

Figure 3

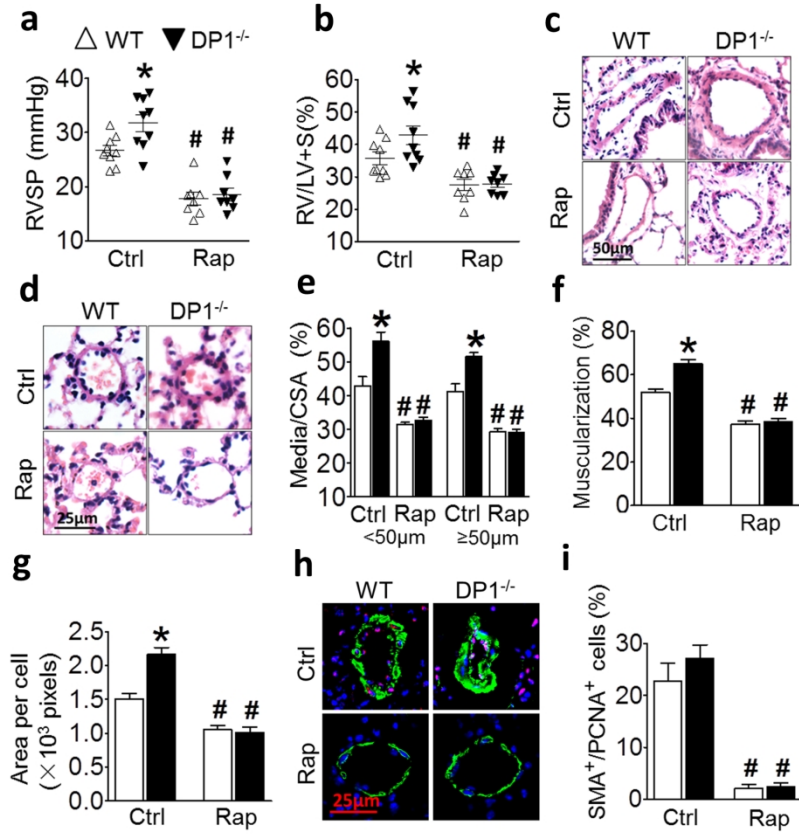


190x253mm (300 x 300 DPI)



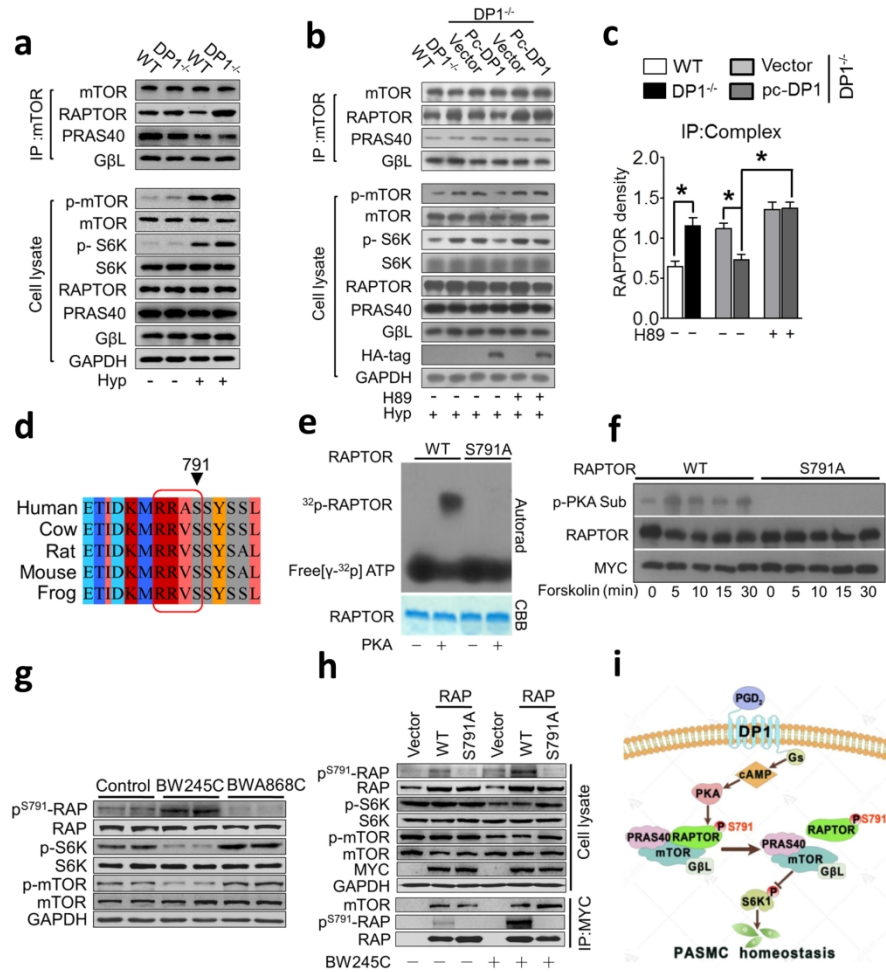
190x253mm (300 x 300 DPI)

Figure 5



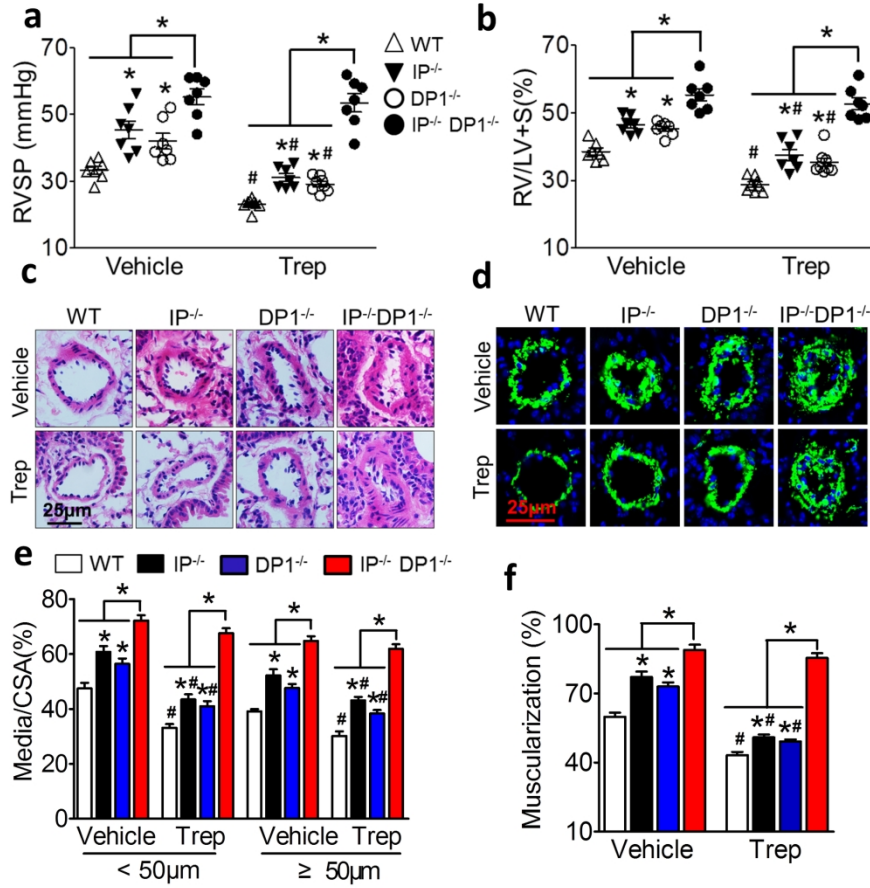
190x253mm (300 x 300 DPI)

Figure 6



190x253mm (300 x 300 DPI)

Figure 7



190x253mm (300 x 300 DPI)

Online Supplemental Materials

Loss of DP1 Aggravates Vascular Remodeling in Pulmonary Arterial Hypertension via mTORC1 Signaling

Yuhu He*, Caojian Zuo*, Daile Jia*, Peiyuan Bai*, Deping Kong*, Di Chen*, Guizhu Liu, Juanjuan Li, Yuanyang Wang, Guilin Chen, Shuai Yan, Bing Xiao, Jian Zhang, Linjuan Piao, Yanli Li, Yi Deng, Bin Li, Philippe P. Roux, Katrin I. Andreasson, Richard M Breyer, Yunchao Su, Jian Wang[†], Ankang Lyu[†], Yujun Shen[†], Ying Yu[†]

Methods

Study approval

Human lung specimens were obtained from patients undergoing lung transplantation for treatment of idiopathic PAH and from unused donor lungs. Patient identifiers were concealed. Waiver of informed consent of human lung samples was approved by the Institutional Review Board (IRB) of the Augusta University, and by the Pulmonary Hypertension Breakthrough Initiative (PHBI) and IRB of the Institute for Nutritional Sciences, Shanghai Institutes for Biological Sciences, Chinese Academy of Sciences.

Reagents

BW245C, BWA868C, H-89, and wortmannin were obtained from Cayman Chemical (Ann Arbor, MI, USA). SU5416, monocrotaline, and rapamycin were purchased from Sigma-Aldrich (St. Louis, MO, USA). Treprostinil was supplied by United Therapeutics Corp. (Research Triangle Park, NC, USA). The raptor and raptor S791A peptides were synthesized by GL Biochem (Shanghai, China).

Lung histology

After hemodynamic measurements, lungs were perfused with PBS and fixed in 10% formaldehyde for 24 h before embedding in paraffin. Sections cut at a thickness of 5 μ m were stained with hematoxylin and eosin for histological analysis. Masson's trichrome staining (Sigma-Aldrich) was performed according to standard procedures. Pulmonary vascular remodeling was quantified by measuring medial wall thickness and percent muscularization.

For the former, 15–20 muscular arteries from each lung categorized as 20–50 or 50–100 μm in diameter were randomly outlined by an observer blinded to mouse genotype or pharmacological treatment. The degree of medial wall thickness—expressed as the ratio of medial area to cross sectional area (medial/CSA)—was analyzed with ImageJ software (National Institutes of Health, Bethesda, MD, USA)(1). To evaluate the degree of muscularization, 30–50 intra-acinar vessels in each mouse with a size between 20 and 50 μm were categorized as non-muscular or partially or fully muscular. PA muscularization is presented as the percentage of partially and fully muscularized pulmonary vessels in total pulmonary vessels(2). Pulmonary vessel cell area was calculated as previously described(3).

PG extraction and analysis

Lung tissue was homogenized and centrifuged, and the supernatant (500 μl) was collected for PG extraction after protein quantification as previously described(4). Briefly, after adding an internal standard, citric acid, and butylated hydroxytoluene, samples were vigorously vortexed with 1 ml of solvent (normal hexane:ethyl acetate, 1:1) for 1 min, then centrifuged at $6000 \times g$ for 10 min. The supernatant (organic phase) was collected and dried under a gentle stream of nitrogen and dissolved in 100 μl of 10% acetonitrile in water. Prostanoid metabolites were quantitated by liquid chromatography–tandem mass spectrometry. PG level was normalized to total protein concentration.

Cell culture

Primary mouse (m)PASMCs were isolated and cultured as previously described(1). Briefly, a segment of proximal PA was isolated under aseptic conditions. After removing adherent fat,

connective tissue, and endothelial cells, the tunica media of the vessels was cut into small pieces (1–2 mm²) and covered with an autoclaved glass cover slip. The PASMCs were cultured in Dulbecco's Modified Eagle's Medium (DMEM) F-12 supplemented with 20% fetal bovine serum (FBS), 100 U/ml penicillin, 2 mM L-glutamine, and 0.1 mg/ml streptomycin (Invitrogen, Carlsbad, CA, USA). Cultured PASMCs were used between passages 3 and 6. Human PASMCs (Number: PCS-100-023) and mouse aortic smooth muscle cells (MOVAS, Number: CRL-2797TM) were purchased from American Type Culture Collection (Manassas, VA, USA.). For hypoxia exposure in vitro, PASMCs seeded in culture dishes were subjected placed in a hermetic tank containing 3% O₂/5% CO₂.

RNA extraction and real-time PCR

Total RNA was isolated from lung tissues, PAs, and PASMCs using TRIzol reagent (Invitrogen) according to the manufacturer's instructions, and 1 µg was reverse transcribed to cDNA using the Reverse Transcription Reagent kit (Takara, Dalian, China). Real-time PCR was performed with triplicates of each sample in a 20-µl reaction volume with SYBR Green universal PCR mix (Takara). Target gene expression was normalized to the level of actin mRNA. The PCR protocol was as follow: 95°C for 5 min; 40 cycles of 95°C for 30 s, 60°C for 30 s, and 72°C for 30 s; and 72°C for 5 min. PCR products were confirmed as a single band of the expected size on a 2% agarose gel. The primer sequences for PCR are shown in Table E1.

Cell proliferation assay

Counting Kit-8 (Dojindo Laboratories, Kumamoto, Japan) was used to assess cell

proliferation according to the manufacturer's instructions. A cell suspension (100 μ l/well) was pre-incubated in a 96-well plate in a humidified incubator. The absorbance at 450 nm was measured using a microplate reader to generate the growth curve.

Construction of DP1 vector and lentivirus encoding DP1

Mouse *DP1* cDNA was subcloned into pcDNA3.1 and a hemagglutinin (HA) tag was added at the extracellular N terminus. Correct insertion of the DNA fragment was confirmed by sequencing. mPASCs were transiently transfected with pcDNA3.1/DP1 or empty pcDNA3.1 vector using Lipofectamine2000 transfection reagent (Invitrogen) according to the manufacturer's protocol.

To generate a DP1-expressing lentivirus, *DP1* cDNA was subcloned into the green fluorescent protein (GFP) expression vector FG12, and the recombinant FG12 vector was co-transfected with pMDLg/pRRE, pRSV-Rev, and pHCMVG into HEK 293T cells. The culture supernatant containing the virus was collected 72 h later. A lentivirus generated from the empty vector was used as the negative control.

In vitro kinase assay

The in vitro kinase assay was performed as previously described(5). To measure raptor phosphorylation by PKA, raptor and raptor S791A peptides (10–20 μ g) were added to buffer composed of 50 mM Tris-Cl (pH 7.4), 10 mM MgCl₂, 2 mM dithiothreitol, 0.1 mM EDTA, 0.01% Brij35, 200 μ M ATP, and 20 mCi [*g*-³²P]ATP (Amersham Pharmacia Biotech, Piscataway, NJ, USA). For the PKA assay, 0.5 U of the catalytic subunit of PKA (New

England Biolabs, Hertfordshire, UK) was added per reaction. Kinase reactions were carried out at 30°C for 30 min and terminated by adding sodium dodecyl sulfate–polyacrylamide gel electrophoresis (SDS–PAGE) loading buffer. Proteins were resolved by Tricine-SDS–PAGE and ³²P-labeled fusion proteins were detected with a Molecular Dynamics phosphorimager (GE Healthcare, Sunnyvale, CA, USA).

Traction force microscopy

Contractile force produced by mPASCs was measured by traction force microscopy as previously described(3, 6). Briefly, fluorescent microbead-embedded elastic gels were treated with *N*-sulfosuccinimidyl-6-(4'-azido-2'-nitrophenylamino) hexanoate (0.5 mg/ml; Pierce, Rockford, IL, USA) and activated by 365 nm ultraviolet irradiation for 10 min, then immediately incubated overnight at 37°C with 100 µg/ml type I collagen (Santa Cruz Biotechnology, Santa Cruz, CA, USA) for cell culture. Cells were maintained under hypoxia (3%) or normoxia (21%) for 24 h.

Measurement of cellular cyclic (c)AMP levels

At about 70% confluence, mPASCs in 12-well plates were cultured overnight in DMEM F-12 containing 2% FBS, and then pre-treated with the phosphodiesterase inhibitor 3-isobutyl-1-methylxanthine (1 mM) for 30 min, followed by incubation with the DP1 agonist BW245C (0.5 µM) and forskolin (1 µM) or vehicle for another 30 min. The cells were washed with cold PBS and then harvested in ice-cold lysis buffer on ice. cAMP level was measured using a cAMP Parameter Assay Kit (R&D Systems, Minneapolis, MN, USA) according to the manufacturer's instructions.

Co-immunoprecipitation

Cell lysates containing 1 mg of protein were incubated with anti-mTOR antibody (1:100; Santa Cruz Biotechnology, cat: sc-517464) or anti-MYC antibody (1:1000; Proteintech, Chicago, IL, USA, cat: 60003-2-1-g) at 4°C for 3 h, followed by overnight incubation with gentle agitation at 4°C with protein A/G agarose (Invitrogen). After extensive washing, immune complexes were recovered by boiling in loading buffer and then subjected to western blot analysis with antibodies against mTOR, raptor(cat: 2280), proline-rich AKT substrate of 40 kDa (PRAS40, cat: 2691), G protein beta subunit-like (GβL, cat: 3274), anti-HA(cat:37245), anti-FLAG(cat:147935), (all diluted 1:1000 and from Cell Signaling Technology, Danvers, MA, USA), and phosphorylated (p-)raptor (1:1000; ABclonal, Wuhan, China, cat: AP0868).

RNA interference

Mouse MOVAS cells (ATCC® CRL-2797™) were cultured in 12-well plates for siRNA transfection by Lipofectamine™ 2000 reagent (Invitrogen) with the 70–80% confluence according to the manufacturer's instructions. In brief, siRNA(2 μg) and Lipofectamine™ 2000 (4μl) were mixed and incubated for 20-30 min at room temperature to allow formation of transfection complexes before delivery on the cells. 48–72 h after interference, the cells were collected to assess the knockdown efficiency and indicated genes expression by qRT-PCR. As for hypoxic condition, cells were exposed to 3% O₂ after siRNA transfection for 6 hours. All the sequences of siRNA (Genepharma, Shanghai, China) used were listed in Table E2.

Prediction of Transcription Factor Binding Sites

The fragment between -4000 and +100 bp of the transcription start site of the DP1 gene from the Eukaryotic promoter (EPD) database was analyzed for putative HIF1 α , Creb1, BCL6 and Egr1 motifs in JASPAR Core (2018 version) using FindM software. A match score with a p value <0.001 was considered to be a high confidence binding site prediction.

Luciferase Assay

The coding sequences of mouse HIF1 α and BCL6 were subcloned into pcDNA3.1 vector (Life Technologies). The mouse DP1 promoter region (0 to -4000 nucleotides) was subcloned into pGL3-Basic plasmid (Promega). HEK293-T cells were cultured in 24-well plates and transfection was performed using the LipofectamineTM 2000 reagent (Invitrogen) with the 70–80% confluence. Cells were co-transfected with 10 ng of the pRL-TK vector DNA (Promega) and 200 ng of HIF1 α or BCL6 expression plasmids and 200 ng of the empty pGL3-Basic plasmid or pGL3-Basic plasmid containing DP1 promoter region. After 24 h incubation, cells were harvested and luciferase activity was measured using the dual luciferase reporter assay system (Promega). Promoter activity is quantified and normalized to the activity of the co-transfected pRL-TK reporter gene.

Chromatin Immunoprecipitation

Mouse MOVAS cells were seeded in 15cm dishes and grown to 70–80% confluence. Cells were then incubated in normoxia or hypoxia for 72 hours. A ChIP assay was performed with a Magna ChIPTM A/G chromatin immunoprecipitation kit (Merck KGaA, Darmstadt,

Germany. Cat: 17-10085) according to the manufacturer's protocol. Briefly, cells were fixed with 1% formaldehyde/PBS and the reaction was stopped by the addition of glycine followed by PBS washing. The pellet was lysed and the chromatin was sheared into 200–1000-bp fragments by sonication. The chromatin extract was incubated with rabbit anti-HIF1 α antibody or anti-BCL6 antibody (Cell Signaling Technology) or rabbit IgG control (ABclonal) at 4 °C with rotation for overnight. The conjugated beads were washed and eluted, and the cross links were reversed by incubation in the presence of proteinase K at 65 °C for 4 h. After purification, DNA was dissolved in elution buffer, and used for quantitative PCR analysis. PCR primers were designed to span individual HIF1 α or BCL6 binding motif (Table E3).

Immunofluorescence analysis

Frozen sections (8 μ m thick) from tissues or glass coverslips with cells were fixed in cold acetone and washed with PBS. After permeabilization with PBS containing 0.25% Triton X-100 for 10 min, samples were incubated with 3% bovine serum albumin in PBS for 30 min to block non-specific antibody binding, then incubated overnight at 4°C with primary antibodies against alpha smooth muscle actin (α -SMA) (1:400; Sigma-Aldrich); proliferating cell nuclear antigen (PCNA) (1:200; Cell Signaling Technology); p-mTOR (1:200) and GFP (1:1000) (both from Abcam, Cambridge, MA, USA); cluster of differentiation (CD)11b (1:400; BD Pharmingen, San Diego, CA, USA); CD68 (1:400; ABD Serotec, Puchheim, Germany) and fibronectin (1:200; Epitomics, Burlingame, CA, USA), followed by three washes with PBS and incubation with Alexa Fluor 488- or Alexa Fluor 594-conjugated

secondary antibody (Invitrogen) for 2 h at room temperature. ProLong Gold antifade reagent with 4',6-diamidino-2-phenylindole (Invitrogen) was used to mount and counterstain the specimens, which were subsequently examined using an LSM 510 laser scanning confocal microscope (Carl Zeiss, Oberkochen, Germany).

Western blotting

Proteins from cell and tissue samples were extracted with lysis buffer containing protease inhibitors. Total protein concentration was determined with the bicinchoninic acid (BCA) method using the BCA Protein Assay Kit (Pierce). Lysates containing equal amounts of protein were separated by 10% or 8% SDS-PAGE and electrotransferred to a polyvinylidene difluoride membrane (Millipore, Billerica, MA, USA). The membrane was blocked in 5% milk in Tris-buffered saline (150 mM NaCl, 50 mM Tris [pH 7.4]) with 0.1% Tween 20 and incubated overnight at 4°C with primary antibodies against the following proteins: collagen and fibronectin (both diluted 1:1000 and from Cayman Chemical); α -SMA (1:1000, Sigma-Aldrich), mTOR and p-mTOR, ribosomal protein S6 kinase (S6K), p-S6K, AKT, p-AKT (Ser473), p-AKT (Thr308), PRAS40, p-PRAS40, 5' AMP-activated protein kinase (AMPK), p-AMPK, extracellular signal-regulated protein kinase (ERK)1/2, p-ERK1/2, p-PKA substrate (RRXS*/T*), p38, p-p38, c-Jun N-terminal kinase (JNK), p-JNK, G β L, raptor, p-raptor (Ser792), HA, Flag, α -tubulin, glyceraldehyde 3-phosphate dehydrogenase (all diluted 1:1000 and from Cell Signaling Technology); and p-raptor (Ser791) (1:1000; ABclonal). The membrane was incubated with appropriate horseradish peroxidase-conjugated secondary antibodies (1:2000; Cell Signaling Technology) in blocking

buffer for 2 h at room temperature, and immunoreactivity was detected by enhanced chemiluminescence (Pierce). Densitometric quantification of protein bands was performed using ImageJ software.

References

1. Lu A, Zuo C, He Y, Chen G, Piao L, Zhang J, Xiao B, Shen Y, Tang J, Kong D, Alberti S, Chen D, Zuo S, Zhang Q, Yan S, Fei X, Yuan F, Zhou B, Duan S, Yu Y, Lazarus M, Su Y, Breyer RM, Funk CD. EP3 receptor deficiency attenuates pulmonary hypertension through suppression of Rho/TGF-beta1 signaling. *J Clin Invest* 2015; 125: 1228-1242.
2. Mouraret N, Marcos E, Abid S, Gary-Bobo G, Saker M, Houssaini A, Dubois-Rande JL, Boyer L, Boczkowski J, Derumeaux G, Amsellem V, Adnot S. Activation of lung p53 by Nutlin-3a prevents and reverses experimental pulmonary hypertension. *Circulation* 2013; 127: 1664-1676.
3. Fredenburgh LE, Liang OD, Macias AA, Polte TR, Liu X, Riascos DF, Chung SW, Schissel SL, Ingber DE, Mitsialis SA, Kourembanas S, Perrella MA. Absence of cyclooxygenase-2 exacerbates hypoxia-induced pulmonary hypertension and enhances contractility of vascular smooth muscle cells. *Circulation* 2008; 117: 2114-2122.
4. Zhang J, Zou F, Tang J, Zhang Q, Gong Y, Wang Q, Shen Y, Xiong L, Breyer RM, Lazarus M, Funk CD, Yu Y. Cyclooxygenase-2-derived prostaglandin E(2) promotes injury-induced vascular neointimal hyperplasia through the E-prostanoid 3 receptor. *Circ Res* 2013; 113: 104-114.
5. Virdee K, Parone PA, Tolkovsky AM. Phosphorylation of the pro-apoptotic protein BAD on serine 155, a novel site, contributes to cell survival. *Curr Biol* 2000; 10: 1151-1154.
6. Xiao B, Gu SM, Li MJ, Li J, Tao B, Wang Y, Zuo S, Shen Y, Yu Y, Chen D, Chen G, Kong D, Tang J, Liu Q, Chen DR, Liu Y, Alberti S, Dovizio M, Landolfi R, Mucci L, Miao PZ, Gao P, Zhu DL, Wang J, Li B, Patrignani P. Rare SNP rs12731181 in the miR-590-3p Target Site of the Prostaglandin F2alpha Receptor Gene

Confers Risk for Essential Hypertension in the Han Chinese Population. *Arterioscler Thromb Vasc Biol*

2015; 35: 1687-1695.

Supplemental Figure Legends

Figure E1. PG profile of lungs from WT and DP1^{-/-} mice after chronic hypoxia exposure. (a) PGD₂, (b) PGE₂, (c) PGF_{2α}, (d) TxA₂, and (e) 6-keto-PGF_{1α}, a stable hydrolyzed product of PGI₂, in lung tissues from WT and DP^{-/-} mice after 3 weeks of hypoxic exposure. #P < 0.05 vs. normoxia (n = 5-6). Data represent mean ± SEM. Statistical significance was evaluated by two-way analysis of variance with Bonferroni post-hoc analysis.

Figure E2. Knockdown of HIF1α or BCL6 prevents hypoxia-induced DP1 downregulation in mouse VSMCs. (a) Relative mRNA levels of DP1 in mouse VSMC line MOVAS in response to hypoxia (Hyp). *P < 0.05 vs. normoxia (Nor) (n = 6). (b) Predicted binding elements of HIF1α, Creb1, BCL6 and Egr1 in the mouse DP1 gene promoter. (c-f) Relative mRNA levels of HIF1α, Creb1, BCL6 and Egr1 in MOVAS cells in response to hypoxia, respectively. *P < 0.05 vs. normoxia (n = 4-6). (g, h) Effect of HIF1α knockdown(g) on DP1 expression in MOVAS cells in response to hypoxia(h). *P < 0.05 vs. normoxia, #P < 0.05 vs. scramble(n=4-6). (i, j) Effect of Creb1 knockdown(i) on DP1 expression in MOVAS cells in response to hypoxia(j). *P < 0.05 vs. normoxia, #P < 0.05 vs. scramble(n=5-6). (k, l) Effect of BCL6 knockdown(k) on DP1 expression in MOVAS cells in response to hypoxia(l). *P < 0.05 vs. normoxia, #P < 0.05 vs. scramble(n=4-6). (m, n) Effect of Egr1 knockdown(m) on DP1 expression in MOVAS cells in response to hypoxia(n). *P < 0.05 vs. normoxia(n=5-6). Data represent mean ± SEM. Statistical significance was evaluated by the two-tailed Student's t test or two-way analysis of variance with Bonferroni post-hoc analysis.

Figure E3. Hypoxia suppresses DP1 expression in mouse VSMCs through HIF1 α /BCL6 complex.(a) Schematic of the mouse DP1 promoter showing the location of HIF1 α (red) and BCL6 (blue) potential binding sites. (b) ChIP analysis of HIF1 α binding capacity in the mouse DP1 promoter in MOVAS cells (n = 6). (c) ChIP analysis of BCL6 binding sites in the mouse DP1 promoter in MOVAS cells (n = 4-6). (d, e) The HIF1 α and BCL6 interaction was analyzed by anti-HA (d) and anti-FLAG (e) immunoprecipitation. (f) Schematic diagram of hypoxia-induced DP1 downregulation in VSMCs through HIF1 α -mediated BCL6 recruitment on DP1 promoter. Data represent mean \pm SEM. Statistical significance was evaluated by two-way analysis of variance with Bonferroni post-hoc analysis.

Figure E4. DP1 deficiency aggravates hypoxia-induced PAH and PA remodeling in mice. (a) RVSP in DP1^{-/-} and WT mice after exposure to hypoxia. *P < 0.05 vs. WT; #P < 0.05 vs. normoxia (n = 8–12). (b) RV/LV+S in DP1^{-/-} and WT mice after exposure to hypoxia. *P < 0.05 vs. WT mice; #P < 0.05 vs. normoxia (n = 8–12). (c, d) Representative hematoxylin and eosin-stained sections of small PAs and arterioles from hypoxia-treated DP1^{-/-} and WT mice. Scale bars: 50 and 25 μ m, respectively. Representative immunofluorescence images of α -SMA (green) expression in small PAs (e) and arterioles (f) from hypoxia-treated DP1^{-/-} and WT mice. Scale bars: 50 and 25 μ m, respectively. (g) Quantification of the ratio of vascular medial thickness to total vessel size for the hypoxia treatment model. *P < 0.05 vs. WT; #P < 0.05 vs. normoxia (n = 8–12). (h) Proportion of partially and fully muscularized PAs (diameter: 20–50 μ m) in hypoxia-treated mice. *P < 0.05 vs. WT; #P < 0.05 vs. normoxia (n = 8–12). (i) Quantification of PASMC size in PAs from hypoxia-treated DP1^{-/-} and WT mice. *P < 0.05 vs. WT; #P < 0.05 vs. normoxia (n = 8

or 9). (j, k) α -SMA gene and protein levels in lungs of hypoxia-treated DP1^{-/-} and WT mice. *P < 0.05 vs. WT; #P < 0.05 vs. normoxia (n = 5). Data represent mean \pm SEM. Statistical significance was evaluated by two-way analysis of variance with Bonferroni post-hoc analysis.

Figure E5. Effect of DP1 deficiency on extracellular matrix deposition in lung tissue in WT and DP^{-/-} mice after chronic hypoxia exposure. (a) Masson's trichrome staining of lung tissue from WT and DP1^{-/-} mice after chronic hypoxia exposure. Scale bar: 50 μ m. (b) Immunofluorescence detection of fibronectin (FN) (red) expression in lung tissue from WT and DP1^{-/-} mice after chronic hypoxia exposure. Scale bar: 50 μ m. (c) Western blot analysis of extracellular matrix protein expression in lung tissue from WT and DP1^{-/-} mice after chronic hypoxia exposure.

Figure E6. Genetic disruption and pharmacological inhibition of DP1 promote PASMC hypertrophy and proliferation in response to hypoxia in vitro. (a) Representative immunofluorescence images of α -SMA (green) expression in WT and DP1^{-/-} PASMCs after normoxia or hypoxia treatment. Scale bar: 25 μ m. (b) Quantification of PASMC size in panel A. *P < 0.05 vs. WT; #P < 0.05 vs. normoxia (n = 17–20). (c) Quantification of the ratio of protein/DNA in WT and DP1^{-/-} PASMCs after normoxia or hypoxia treatment. *P < 0.05 vs. WT. #P < 0.05 vs. normoxia (n = 5). (d) Representative immunofluorescence images of α -SMA (green) expression in human PASMCs treated with BWA868C (10 μ M) after normoxia or hypoxia exposure. Scale bar: 25 μ m. (e) Quantification of PASMC size in panel D. *P < 0.05 vs. vehicle. #P < 0.05 vs. normoxia (n = 17–20). (f) Quantification of the ratio of

protein/DNA in hypoxia-challenged human PASMCs after BWA868C treatment. *P < 0.05 vs. vehicle. #P < 0.05 vs. normoxia (n = 6). (g) Proliferation of cultured WT and DP1^{-/-} PASMCs in response to hypoxia. *P < 0.05 vs. vehicle (n = 6). (h) Proliferation of cultured BWA868C-treated human PASMCs in response to hypoxia. *P < 0.05 vs. vehicle (n = 6–9). (i) Representative immunofluorescence images of α -SMA (green) and PCNA (red) expression in lung sections of WT and DP1^{-/-} mice after chronic hypoxia exposure. Scale bar: 25 μ m. (j) Quantification of SMA- and PCNA-positive cells in panel I. #P < 0.05 vs. normoxia (n = 5). Data represent mean \pm SEM. Statistical significance was evaluated by two-way analysis of variance with Bonferroni post-hoc analysis.

Figure E7. Effect of DP1 deficiency on perivascular inflammatory response in lungs of mice with hypoxia-induced PAH. (a, b) Representative immunofluorescence images of CD11b (a, red) and CD68 (b, red) expression in lung tissues from DP1^{-/-} and WT mice after chronic hypoxia exposure. Scale bar: 50 μ m.

Figure E8. Effect of EP2 deficiency on development of hypoxia-induced PAH in mice. (a, b) RVSP and RV/LV+S ratio in EP2^{-/-} and WT mice after chronic exposure to hypoxia. #P < 0.05 vs. normoxia (n = 6–8). (c) Representative images of hematoxylin and eosin-stained lung sections from normoxia- or hypoxia-treated WT and EP2^{-/-} mice. Scale bar: 50 μ m. (d) Quantification of the ratio of vascular medial thickness to total vessel size in panel C. #P < 0.05 vs. normoxia (n = 6–8). Data represent mean \pm SEM. Statistical significance was evaluated by two-way analysis of variance with Bonferroni post-hoc analysis.

Figure E9. Re-expression of DP1 in lung tissue ameliorates the exacerbated PAH in

hypoxia-treated DP1^{-/-} mice. (a) Representative immunofluorescence images of α -SMA (green) and GFP (red) expression in lung sections of DP1^{-/-} mice transduced with lentivirus encoding GFP-tagged DP1. Scale bar: 25 μ m. (b) mRNA levels of DP1 in lung tissue of mice after transduction with lentivirus expressing DP1. *P < 0.05 vs. vector (n = 4). (c, d) Effect of DP1 re-expression on RVSP and RV/LV+S ratio in hypoxia-treated DP1^{-/-} mice. *P < 0.05 vs. vector (n = 8). (e) Representative hematoxylin and eosin-stained lung tissue sections from DP1^{-/-} mice transduced with lentivirus expressing DP1 after chronic hypoxia exposure. (f–h) Quantification of the ratio of vascular medial thickness to total vessel size (f), proportion of partially and fully muscularized pulmonary arterioles (20–50 μ m in diameter) (g), and quantification of PASMC size (h) in panel e. *P < 0.05 vs. vector (n = 8). Data represent mean \pm SEM. Data were calculated by 2-tailed Student's t test.

Figure E10. Effect of DP1 deficiency on MAPK signaling in cultured mPASMCs exposed to hypoxia.

Figure E11. DP1 deficiency leads to increased mTOR activity in PAs from hypoxia-treated mice. (a) Western blot analysis of activated mTOR signaling components in lung tissue of hypoxia-treated WT and DP1^{-/-} mice. (b) Representative immunofluorescence images of α -SMA (green) and p-mTOR (red) expression in lung sections from hypoxia-treated WT and DP^{-/-} mice. Scale bar: 50 μ m.

Figure E12. Effect of DP1 deficiency on AKT activation in cultured mPASMCs exposed to hypoxia.

Figure E13. Effect of DP1 deficiency on AKT Thr308 and PRAS40 Thr246

phosphorylation levels and PI3K activation in cultured mPASCs in response to hypoxia. (a) Western blot analysis of p-AKT and p-PRAS40 levels in cultured mPASCs exposed to hypoxia or normoxia. (b) Effect of PI3K inhibitor treatment on mTOR signaling in mPASCs re-expressing DP1 after hypoxia exposure.

Figure E14. Effect of DP1 deficiency on AMPK activity (a) and raptor Ser792 phosphorylation (b) in hypoxia-challenged mPASCs.

Figure E15. Rapamycin treatment abolishes the increases in proliferation, hypertrophy, and traction force in cultured DP1^{-/-} mPASCs in response to hypoxia. (a) Effect of rapamycin (20 nM) on the proliferation of cultured mPASCs in response to hypoxia. *P < 0.05 vs. WT (n = 6). (b) Quantification of the ratio of protein/DNA in hypoxia-treated mPASCs with rapamycin treatment. *P < 0.05 vs. WT; #P < 0.05 vs. control (n = 6). (c) Representative phase contrast images and traction stress of hypoxia-treated mPASCs treated with rapamycin. (d) Quantification of the traction force (Pa) in panel c. *P < 0.05 vs. WT; #P < 0.05 vs. control (n = 8–10). Data represent mean ± SEM. Statistical significance was evaluated by two-way analysis of variance with Bonferroni post-hoc analysis.

Figure E16. Western blot analysis of p-raptor (Ser791) expression in forskolin-treated 293T cells expressing myc-tagged WT and S791A mutant raptor.

Figure E17. Treprostinil treatment inhibits mTORC1 activity and downstream S6K phosphorylation in PASCs. (a) Effect of treprostinil (Trep) treatment on mTORC1 signaling in primary human PASCs in response to hypoxia. (b) Representative immunofluorescence images of α -SMA (green) and mTOR (red) expression in lung sections

of HySu-challenged mice after treprostinil treatment. Scale bar: 50 μ m,

Table E1. Primers for PCR

Target	Forward primer (5'–3')	Reverse primer (5'–3')
Human DP1	ATGCGCAACCTCTATGCGAT	GCGCGATAAATTACGGGCAG
Human DP2	CCTCTGTGCCAGAGCCCCACGA TG	CACGGCCAAGAAGTAGGTGAAGA AG
Human GAPDH	AACTTTGGCATTGTGGAAGG	CACATTGGGGGTAGGAACA
Mouse DP1	GCTTTCTGTGCGCTCCCCTTTG	CATCCGGAATACTGAAGTCCTG
Mouse DP2	CAATCTCCCGGAGCAAGGTG	CCAGGTAACCTCCTCGATGGC
Mouse α -SMA	TCCTGACGCTGAAGTATCCGAT	GGCCACACGAAGCTCGTTATAG
Mouse Egr1	TCGGCTCCTTTCCTCACTCA	CTCATAGGGTTGTTTCGCTCGG
Mouse BCL6	CCGGCACGCTAGTGATGTT	TGTCTTATGGGCTCTAAACTGCT
Mouse Creb1	ACCCAGGGAGGAGCAATACAG	TGGGGAGGACGCCATAACA
Mouse HIF1 α	ACCTTCATCGGAAACTCCAAAG	CTGTTAGGCTGGGAAAAGTTAGG
Mouse β -actin	GTACCACCATGTACCCAGGC	AACGCAGCTCAGTAACAGTCC
Mouse GAPDH	CCCTTATTGACCTCAACTACATG GT	GAGGGGCCATCCACAGTCTTCTG
Rat DP1	TGAATGAGTCCTATCGCTGTC	GGTGATGTGCCTTTGGTAGAA
Rat DP2	CTTCCAAACCACAGCAACTC	CAGAGCATCAGGCAGACTC
Rat β -actin	ACGGTCAGGTCATCACTATCG	GGCATAGAGGTCTTTACGGATG

Table E2. siRNA sequences

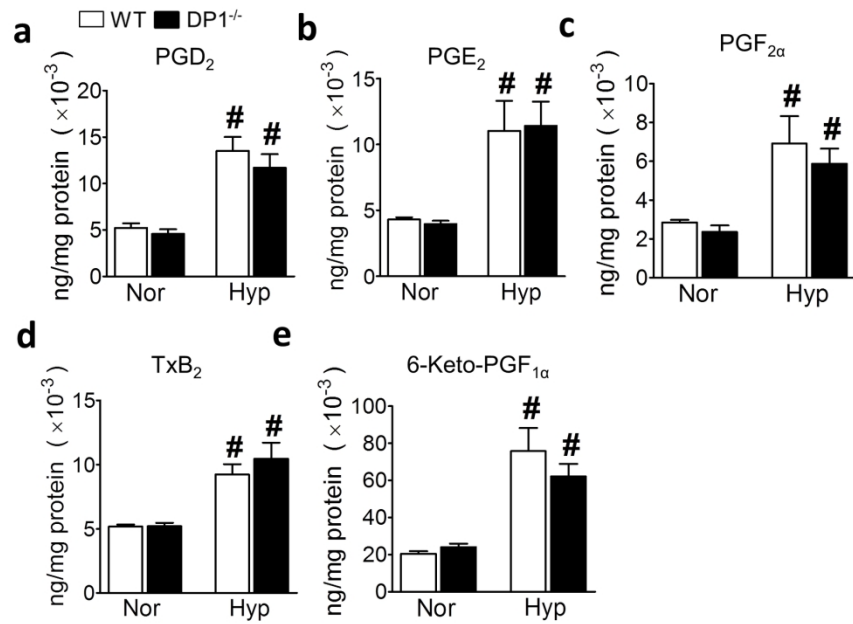
Target	Forward primer (5'–3')	Reverse primer (5'–3')
Mouse		
si-mHIF1 α	CUGAUAACGUGAACAAAUATT	UAUUUGUUCACGUUAUCAGTT
si-mBCL6	GCCUCAAUCAGAAUGCCAATT	UUGGCAUUCUGAUUGAGGCTT.
si-mEgr1	CAGGACUUAAGGCUCUUATT	UAAGAGCCUUUAAGUCCUGTT.
si-mCreb1	GUCUCCACAAGUCCAAACATT	UGUUUGGACUUGUGGAGACTT

Table E3. Predicted binding sites for HIF α and BCL6 on mouse DP1 promoter

Binding sites	Forward primer (5'–3')	Reverse primer (5'–3')
HIF1 α		
1. -3651~ 3636	ACCCCGAAGCCTGAAG ATTG	AGCCCTAAGGAGCAGGA TGA
<i>TGGGAACG</i> TAGTAGA		
BCL6		
1. -461~ -443	ACATGGAAACTTGCAGC TACC	TGGTGTTTTGGTTGCCAC AA
<i>TCTGCCGCTTCCAAAATC</i>		
2. -781~ -763	GTGAGGTCAAAGCAGT CCCA	CAGAGGGCATCAGGGTT CTG
<i>AACTTTCCTCAAATAAAA</i>		
3. -1548~ -1528	CCCCCTTCAGATTCTAC TGCC	AGACTAGTCTCATGTGCA CTTGA
<i>AGAACTTCCTTCCCCTTCCATTC</i>		
4. -1904~ -1885	AACCAGGAGGAAACGT GTGG	ATGAGCTGTGGGACCCA ATG
<i>GTGGTTTCCTTAATTGTAC</i>		
5. -3826~ -3807	GCCAGTTGTTTCAGGGAA GGA	GCCTTGAACGTAACACCT GG
<i>AGGCTTTCCTCCTCCAGGT</i>		

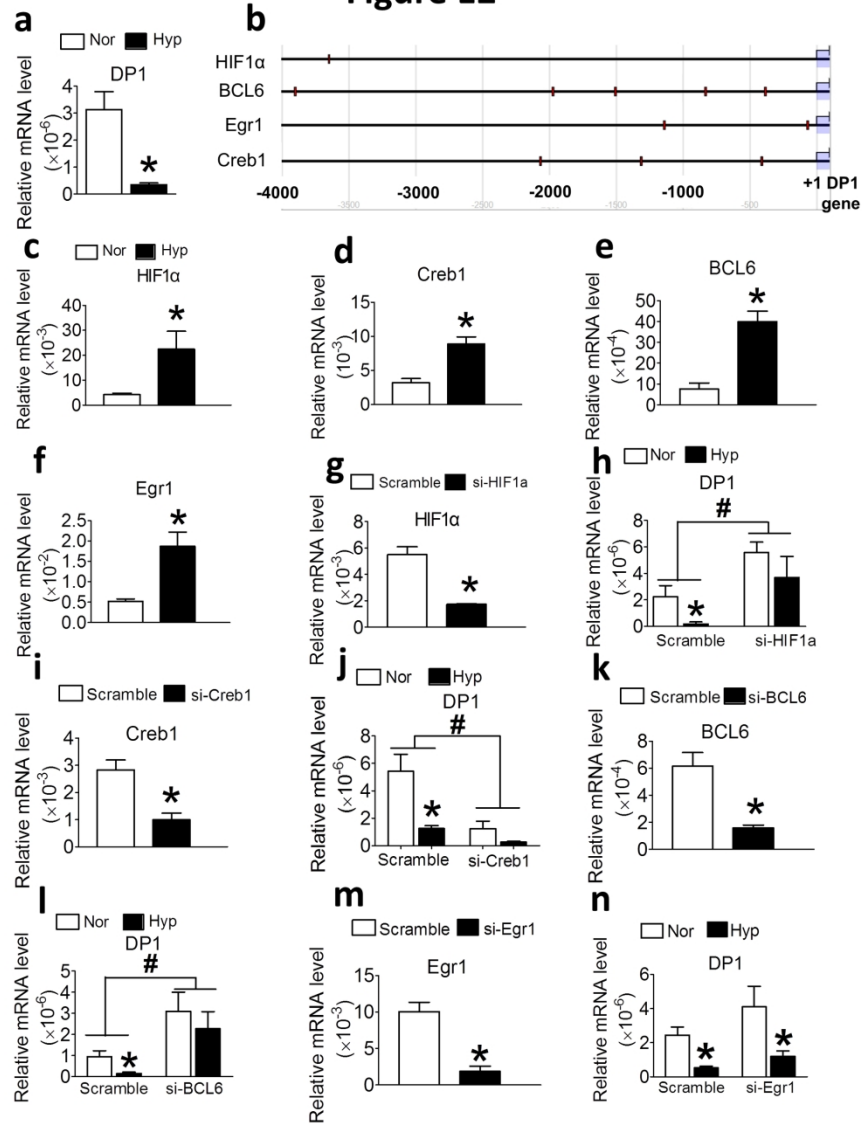
* *Italic scripts* indicate the binding motif.

Figure E1



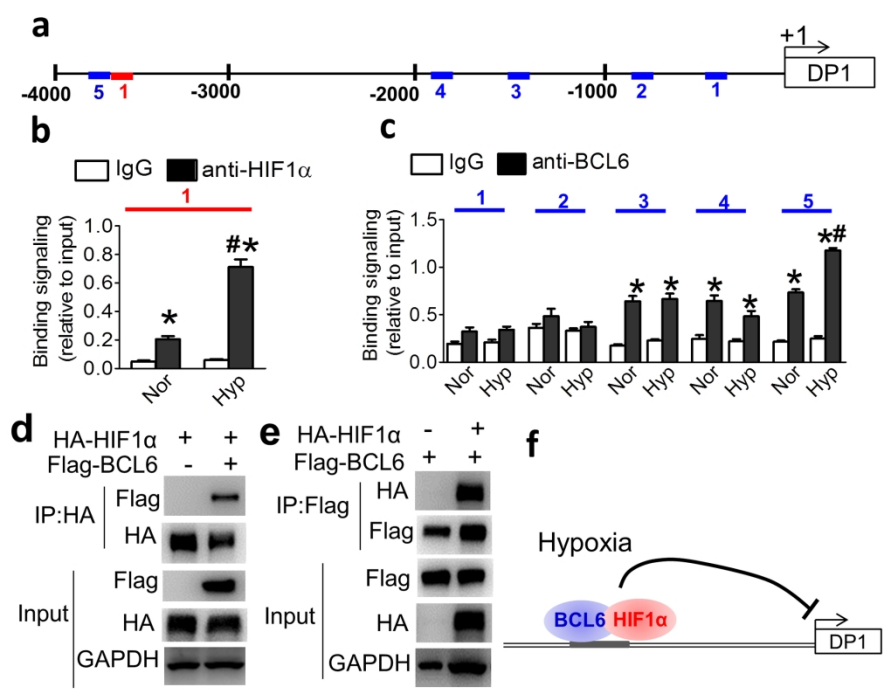
190x253mm (300 × 300 DPI)

Figure E2



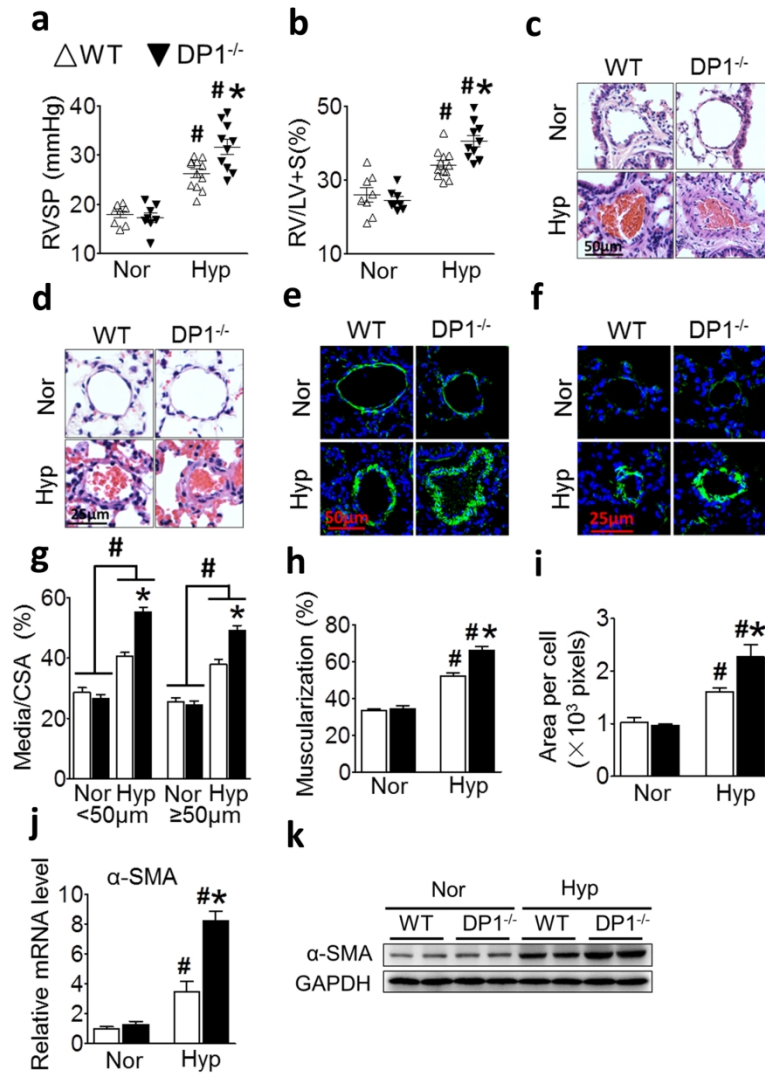
190x253mm (300 x 300 DPI)

Figure E3

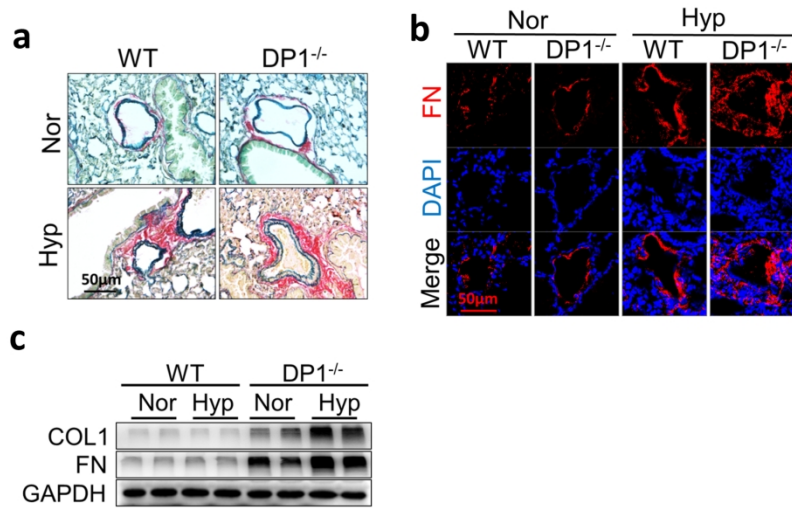


190x253mm (300 x 300 DPI)

Figure E4

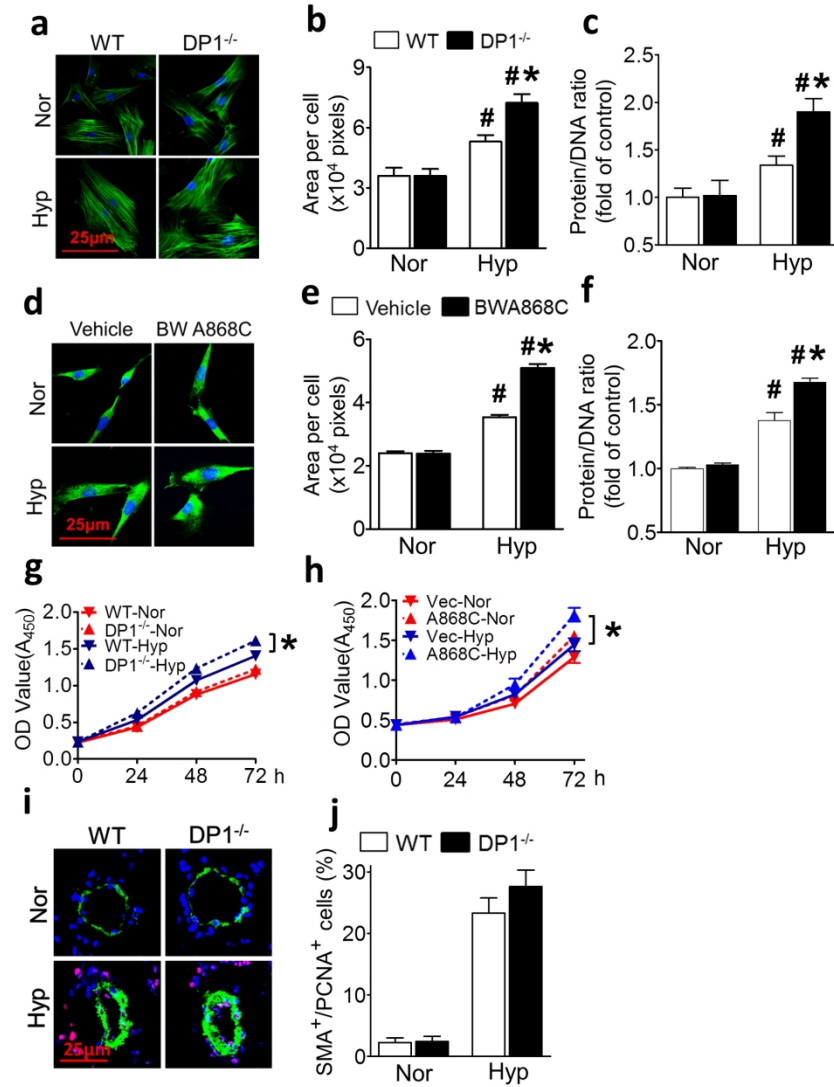


190x253mm (300 x 300 DPI)

Figure E5

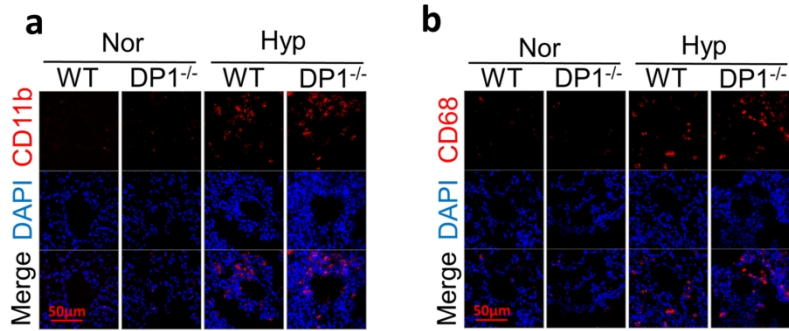
190x253mm (300 x 300 DPI)

Figure E6



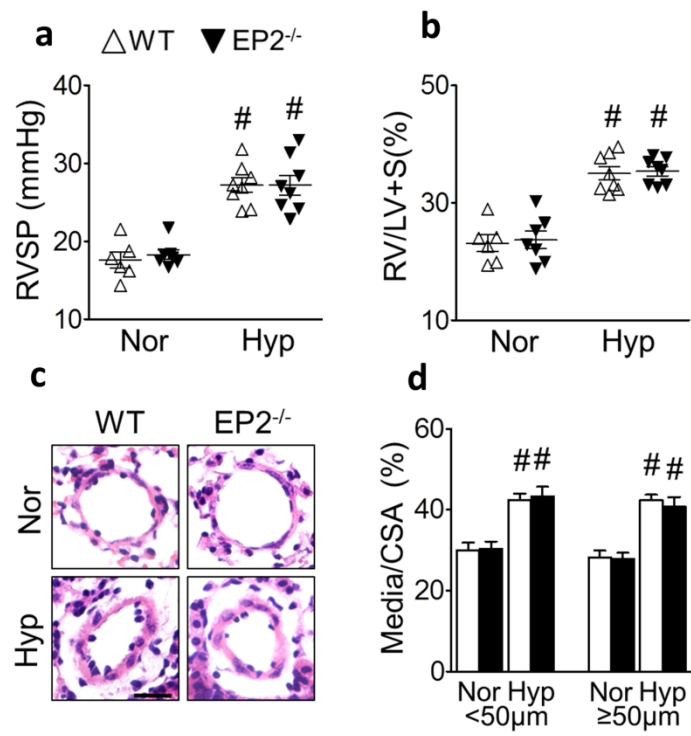
190x253mm (300 x 300 DPI)

Figure E7



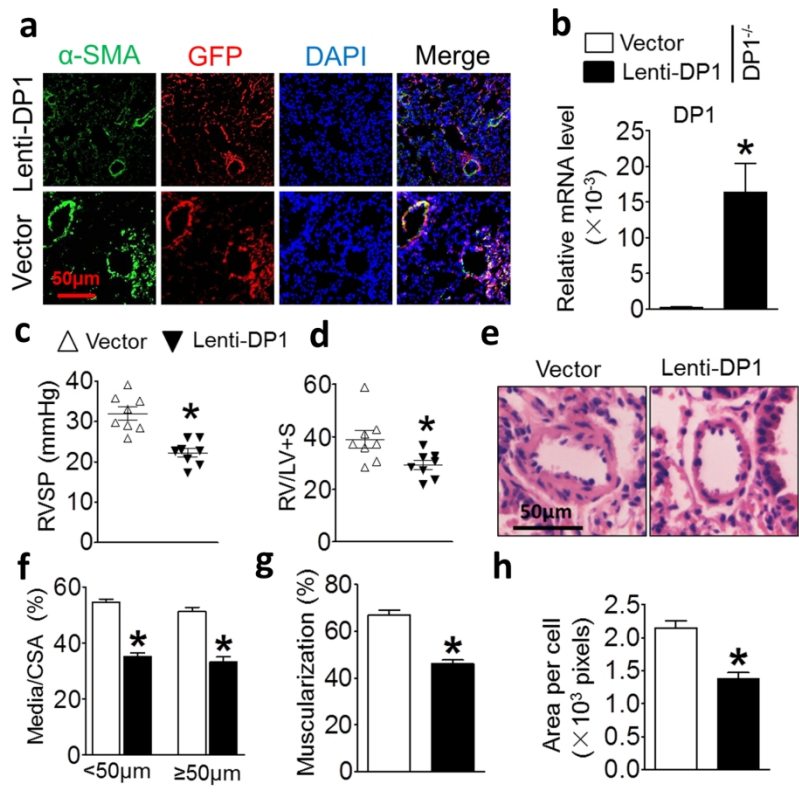
190x253mm (300 x 300 DPI)

Figure E8

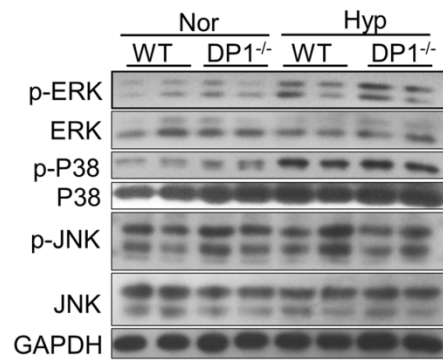


190x253mm (300 x 300 DPI)

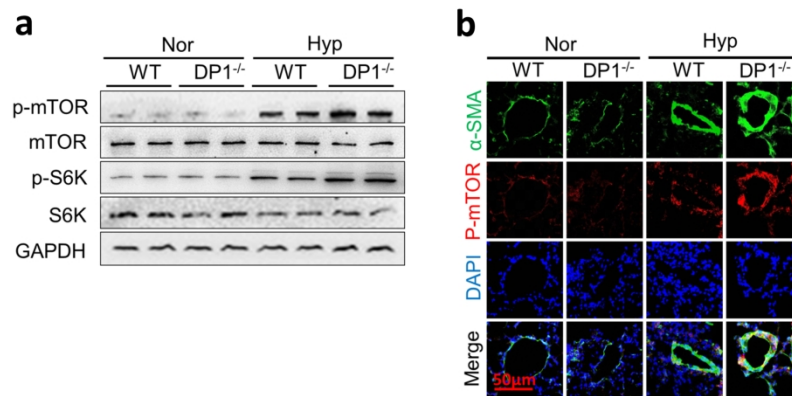
Figure E9



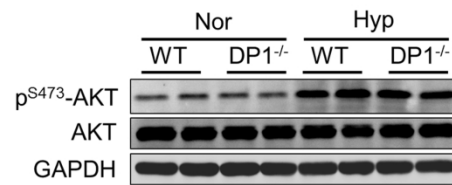
190x253mm (300 x 300 DPI)

Figure E10

190x253mm (300 x 300 DPI)

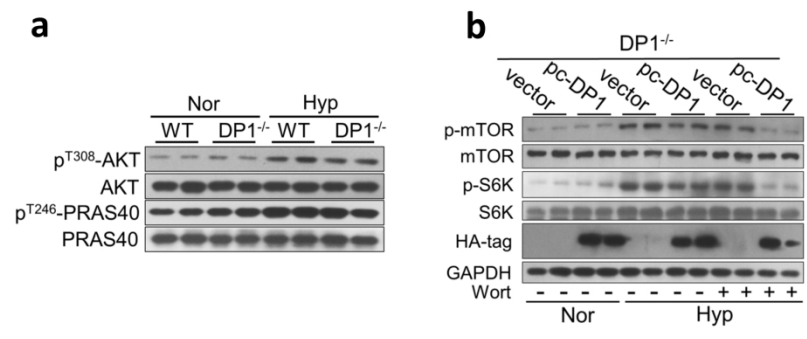
Figure E11

190x253mm (300 x 300 DPI)

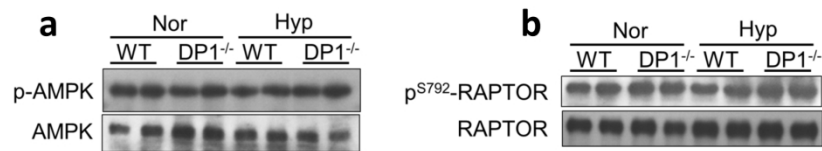
Figure E12

190x253mm (300 x 300 DPI)

Figure E13

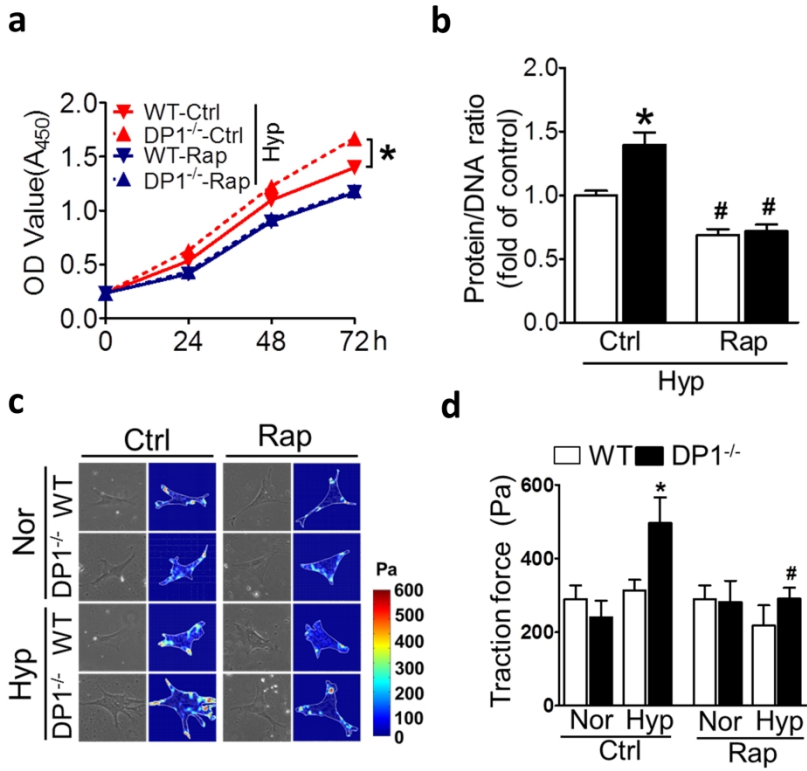


190x253mm (300 x 300 DPI)

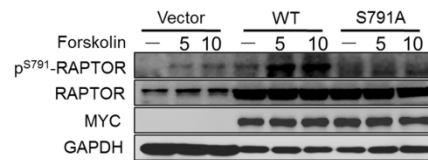
Figure E14

190x253mm (300 x 300 DPI)

Figure E15

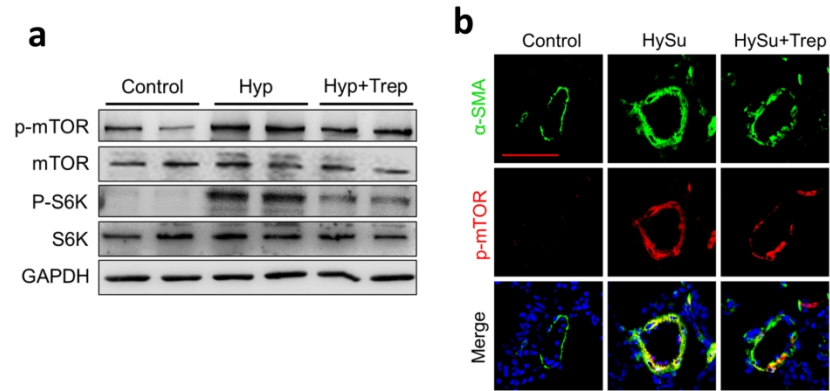


190x253mm (300 x 300 DPI)

Figure E16

190x253mm (300 x 300 DPI)

Figure E17



190x253mm (300 x 300 DPI)